© 2007 International Press
Adv. Theor. Math. Phys. **11** (2007) 839–912

Crosscaps in Gepner models and the moduli space of T^2 orientifolds

Brandon Bates[1], Charles Doran[2,*], and Koenraad Schalm[1,†]

[1]Institute for Strings, Cosmology and Astroparticle Physics, Department of Physics, Columbia University, New York, NY 10027, USA
bdbates@phys.columbia.edu, schalm@science.uva.nl
[2]Department of Mathematics, Columbia University, New York, NY 10027, USA
doran@math.washington.edu

Abstract

We study T^2 orientifolds and their moduli space in detail. Geometrical insight into the involutive automorphisms of T^2 allows a straightforward derivation of the moduli space of orientifolded T^2s. Using $c = 3$ Gepner models, we compare the explicit worldsheet sigma model of an orientifolded T^2 compactification with the CFT results. In doing so, we derive half-supersymmetry preserving crosscap coefficients for generic unoriented Gepner models using simple current techniques to construct the charges and tensions of Calabi–Yau orientifold planes. For T^2s, we are able to identify the O-plane charge directly as the number of fixed points of the involution; this number plays an important role throughout our analysis. At several points we make connections with the mathematical literature on real elliptic curves. We conclude with a preliminary extension of these results to elliptically fibered $K3$s.

e-print archive: http://lanl.arXiv.org/abs/arXiv:hep-th/0612228

*Current address. Department of Mathematics, University of Washington, Seattle, WA 98195, USA

†Current address. Institute for Theoretical Physics, University of Amsterdam, Valckenierstraat 65, Amsterdam 1018XE, The Netherlands

1 Introduction

Orientifolds are mysterious beasts, whose taxonomic classification is starting to come of age. Orientifolds are an important aspect in the study of string theory vacua. As we have become recently aware, the majority of (supersymmetric) vacua are probably of the orientifold type [1, 2]. Generically orientifold compactifications will contain orientifold planes: a non-perturbative "object" in string theory which characteristically can carry negative tension and charge. All compactifications can in fact be organized in superselection sectors determined by their orientifold plane content.

Of phenomenological interest are those string compactifications with $\mathcal{N} = 1$ $d = 4$ supersymmetry. Next to heterotic Calabi–Yau compactifications and M-theory on G_2 manifolds, type II Calabi–Yau compactifications with D-branes (type I Calabi–Yau compactifications) provide a new class. This class has shown promising signs of not only being able to describe cosmological string theories with a period of slow-roll inflation, [3–6], but also contain models with SM-model-like spectra [7]. With the gauge sector descending from D-branes, these compactifications are "brane-world" scenarios. Type I compactifications must obey a consistency condition — tadpole cancellation — which is Gauss's law that the total charge in the internal space vanishes, and supersymmetry dictates that the only compatible "negative" charge object is the orientifold plane. Hence all supersymmetric type II brane compactifications must be orientifolds. For the study of string vacua, it is of great interest to know what the possible orientifold planes are for a Calabi–Yau manifold and their charges with respect to internal gauge-fields.

The mystery of orientifold planes lies in their properties. They can behave as negative tension objects at long range, yet do not violate any GR energy theorems [8, 9]. Perturbatively they have no moduli, which leads to the question whether orientifolds are objects at all. Non-perturbatively they are thought to be a either a (non-dynamical) condensation of D-branes [10–12] or resolve into a smooth geometry [13]. Particularly these last results suggest that orientifold planes are perhaps remnants of purely quantum-geometrical characteristics with no true classical analog, rather in the same way that fermions are intrinsically quantum objects.

Indeed, the main obstacle in our understanding of orientifold planes is that they lack an intrinsic classical geometric description. D-branes are the quantum-geometric version of vector-bundles. Orientifolds, however, as we now know them, are intrinsically defined in perturbative string theory by modding out by a worldsheet parity transformation (times a spacetime involution). This projection will generically also remove a number of geometric moduli. In particular, toroidal orientifold compactifications are

known where the true large volume limit is absent [14]. Consistent with the suggestion above, a classical geometric version of such a compactification does not seem to exist. For others, the large volume limit does exist. This study partly seeks whether some characteristics of orientifold planes may be geometrically determined, especially those characteristics which are relevant to the construction of phenomenologically viable string vacua, namely the location of the planes, their charges and tensions, the effect and relation to the moduli space of the oriented parent theory; and how O-planes behave throughout the moduli space. Because orientifold compactifications are intrinsically defined at the worldsheet level, we will use worldsheet CFT methods to try to extract this information. The systematics of building consistent unoriented CFTs and specifically rational CFTs (RCFTs) are by now well understood [15]. To solve the associated algebraic constraints in practice is computationally involved and may generically only be possible mechanically [7, 16, 17]. A search for a geometrical understanding is motivated by the expectation that geometrical insight will allow analytic insight into consistent orientifold compactifications.

The Gepner construction is the most well-known example of an RCFT description of a Calabi–Yau compactification at a special point in its moduli space. In principle, the construction of unoriented Gepner models has been known for some time (see e.g. [18]); the emphasis on the geometrical aspects is more recent [20–33]. In particular, the two articles by Brunner and Hori, and by Brunner, Hori, Ha and Walcher, (1) show that O-planes are located at fixed points of (anti-)holomorphic isometries, (2) argue that the moduli space is unobstructed and computed the local dimension and (3) in specific examples study the geometry and moduli-space of consistent CY-3-fold orientifolds. In these examples, the charges and tensions of the O-planes are known and canceled by the addition of appropriate D-branes. We study here the simplest non-trivial example in detail: a CY-1-fold or two-torus compactification. The advantage is that throughout the torus moduli-space we have an additional description, aside from the abstract Gepner description and the gauged linear sigma-model description. The worldsheet sigma-model covers the full moduli space rather than a subspace. Furthermore, our approach will differ from the methods of Brunner *et al.* in one subtle detail. Their orbifold CFT results apply to any Gepner model, but they are not extendible to generic RCFTs. In general, one ought to use simple current techniques (see e.g. [34, 35]). We do so here. Simple current techniques for Gepner orientifolds were recently used in [36] and underlie the search for Standard-Model like brane-world compactifications in [7, 16]. We review both the Gepner construction and the unoriented simple current extended RCFTs in Section 3; details are provided in Appendix A. In Section 4, we will use these results to determine the O-plane properties of $c = 3$ Gepner models corresponding to two-torus compactifications. Finally

in Section 5, we compare the results with the exact worldsheet sigma-model description. We conclude with a discussion and outlook on how our torus results may provide insight in elliptically fibered CYs and $K3$s in particular. In terms of the general aim of this study, we will succeed in giving a geometrical description of the charge/tension of A-type O-planes as the number of fixed points of the associated involution. This is a direct extension of the results by Brunner and Hori. This number of fixed points plays a guiding role throughout. Classically it is an invariant. Indeed in Section 2, we begin with a simple geometrical analysis of orientifolds of T^2s by analyzing for which points in the moduli space involutions exist. We will then show how in the moduli space of unoriented T^2s this number of fixed points is a topological obstruction. We conclude in Section 6 with an outlook how the results for T^2 orientifolds may be applied to elliptically fibered families and $K3$s in particular. Curiously, we will show here that the number of fixed points of the T^2 fiber can change in the family. In such fibered surfaces, it is therefore no longer an invariant.

A final result of this article is to connect various mathematical results on real elliptic curves [37–40] with the physics of orientifold compactifications.

2 The geometry of T^2 orientifolds

Geometrically, the most pronounced characteristic of orientifolds is their localization at fixed points of involutive spacetime automorphisms. Given a manifold and its involutive automorphisms, we can decide to restrict our attention to physical states invariant under the action of the involutive automorphisms. If we combine the action of the involutive automorphism with a worldsheet orientation reversal, the fixed point locus of the automorphism is an orientifold plane. String theory, however, tells us that these orientifold planes carry both tension and charges under various p-form potentials on the manifold. To understand these charges from a purely geometric construction is one of the main aims of the recent work on orientifold constructions. A proper understanding will facilitate the construction of consistent orientifold compactifications in particular on Calabi–Yau manifolds (see for example [7, 16]).

To illustrate the power of geometrical insight, we will deduce in this section properties of T^2 orientifolds purely from geometry. The remainder of this article will be devoted to a review and construction of T^2 orientifolds from first principles. They will naturally confirm the geometrical results. We will clearly see the benefits and shortcomings of both methods. The geometrical approach yields us the full moduli space of T^2 orientifolds with little

effort. However, the charges and tensions of the orientifold planes require some work. Fortunately for T^2s it is straightforward and we will show that the O-plane charge is simply related to the number of fixed points of the involution. The string theory approach yields the converse. The charges are explicitly computable but the moduli space is less clear. By an argument of Kapranov and Oh (page 112 [28]) the moduli-space of orientifolds is unobstructed, so that a perturbative analysis in string theory should suffice to find the moduli space as well. For T^2s this does not seem to be the case, as we will show below. In Section 6, we do find evidence that this obstruction is lifted when the T^2 is non-trivially fibered over some base.

2.1 T^2 orientifolds

The complete geometrical data of a T^2 compactification is given by two complex numbers τ and ρ. Consider the torus as $\mathbb{R}^2$ modded out by a lattice Λ generated by two vectors e_1, e_2. Scaling and rotating e_1 to the unit vector $(1,0)$ and reflecting across the horizontal axis if necessary, the complex number τ, $\operatorname{Im}\tau > 0$, is the lattice vector e_2 in $\mathbb{C} \simeq \mathbb{R}^2$. The natural lattice structure implies that

$$\tau \longrightarrow \frac{a\tau + b}{c\tau + d}, \quad \begin{pmatrix} a & b \\ c & d \end{pmatrix} \in \mathrm{PSL}(2,\mathbb{Z}), \tag{2.1}$$

describes the same torus. Geometrically τ classifies the complex structure of the torus. The other complex number ρ is the complexified Kähler class: $\rho = \int_{T_2} B + \mathrm{i}J$. Here $J \sim \sqrt{G}dx \wedge dy$ is the Kähler form parametrizing the size of the torus, and B is the NS–NS two-form. T-duality combined with the gauge symmetry $B \to B + 1$ implies that

$$\rho \longrightarrow \frac{a\rho + b}{c\rho + d}, \quad \begin{pmatrix} a & b \\ c & d \end{pmatrix} \in \mathrm{PSL}(2,\mathbb{Z}), \tag{2.2}$$

also describes the same torus. The quantum moduli space of an elliptic curve is thus given by two copies of the fundamental domain of $\mathrm{PSL}(2,\mathbb{Z})$ (see figure 1) subject to three global $\mathbb{Z}_2$ symmetries: mirror symmetry which exchanges τ with ρ: $(\tau,\rho) \to (\rho,\tau)$, spacetime parity which sends (τ,ρ) to minus their complex conjugates: $(\tau,\rho) \to (-\bar{\tau},-\bar{\rho})$, and worldsheet parity which sends ρ to minus its complex conjugate: $(\tau,\rho) \to (\tau,-\bar{\rho})$ [41].

To consider orientifold compactifications, we need to identify the involutive automorphisms of a T^2. These are easily derived and can also be found in the mathematical literature [37, 38]. Any automorphism of T^2 will, up to a lattice vector, also be an automorphism of the covering space $\mathbb{R}^2$. Using complex coordinates $z = x + \mathrm{i}y$, these divide into holomorphic, $z \to \gamma z + \delta$,

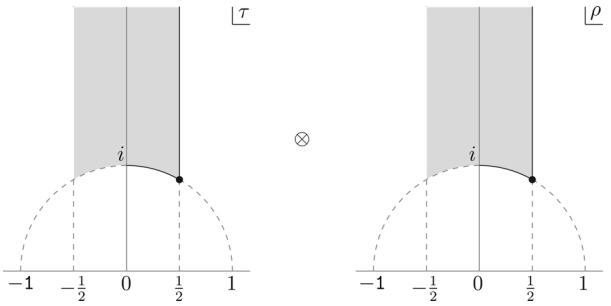

Figure 1: The moduli space of T^2 compactifications: the boundary of the fundamental domain is included when bold.

and anti-holomorphic, $z \to \alpha\bar{z} + \beta$, automorphisms. The $\mathbb{R}^2$ automorphisms are involutions of the torus $T^2 = \mathbb{R}^2/\Lambda$, iff (1) acting once, they return the same torus (i.e., map the lattice vectors to other lattice vectors) and (2) acting twice they return the same point on the torus. The latter requirement tells us that for $\gamma = 1,\ 2\delta = n\tau + m,$ or $\gamma = -1,\ \delta \in \mathbb{C}$ we obtain holomorphic involutions, and for $|\alpha|^2 = 1,\ \alpha\bar{\beta} + \beta = n\tau + m$ we have anti-holomorphic involutions. Without loss of generality, the shifts $\beta \in \mathbb{C}/\Lambda$ can be limited to those within the torus; the unit norm constraint, $|\alpha|^2 = 1$, then implies that β is half a lattice vector: $\beta = (n\tau + m)/2$ with $n, m \in \{0, 1\}$, if $|\beta|^2 = |n\tau + m - \beta|^2$ is to have a solution. For reasons we will explain in Section 3 the latter, i.e., anti-holomorphic involutions, are known as type A and holomorphic ones as type B. Moreover, mirror symmetry maps type A involutions into type B and vice versa.

For anti-holomorphic type A involutions the first requirement is equivalent to demanding that

$$\alpha \cdot 1 = a\tau + b + \beta, \quad a, b \in \mathbb{Z}, \tag{2.3}$$

$$\alpha \cdot \bar{\tau} = c\tau + d + \beta, \quad c, d \in \mathbb{Z}. \tag{2.4}$$

Equation (2.3) states that α is a lattice vector. Suppose $|\tau|^2 > 1$. The condition that α has norm one, then uniquely fixes $\alpha = \pm 1$; all other lattice vectors have norm larger than one. Furthermore, from equation (2.4) we conclude that $\bar{\tau}$ is then also a lattice vector. This implies that $\tau + \bar{\tau} \in \mathbb{Z}$. For τ in the fundamental domain, FD, this has the solutions $\mathrm{Re}(\tau) = 0, (1/2)$. To derive the explicit involution, there are five natural cases to consider

(a) $\tau = \mathrm{i}\tau_2$ with $\tau_2 > 1$ (and $\tau_2 \in \mathbb{R}$). Here $\alpha = \pm 1$. For both values of α all shifts $\beta = 0, \frac{1}{2}, \frac{\mathrm{i}\tau_2}{2}, \frac{\mathrm{i}\tau_2 + 1}{2}$ are compatible with the involution constraint $\alpha\bar{\beta} + \beta = c\tau + d$.

(b) $\tau = \mathrm{i}$. The constraint (2.3) that α be a lattice vector has the solutions $\alpha = \pm 1$ and $\alpha = \pm\mathrm{i}$. The second constraint (2.4) is always satisfied.

Again all shifts β are allowed for $\alpha = \pm 1$. For $\alpha = \pm \mathrm{i}$ only the shifts $\beta = 0, \frac{\mathrm{i}+1}{2}$ are allowed.

(c) $\tau = \exp(\mathrm{i}\theta)$ with $\pi/2 > \theta > \pi/3$. The constraint (2.3) that α be a unit norm lattice vector has solutions $\alpha = \pm 1$ and $\alpha = \pm\tau$. Now, however, the second constraint (2.4) only allows the solution $\alpha = \pm\tau$. As in case (b) this allows the shifts $\beta = 0, \frac{\tau+1}{2}$.

(d) $\tau = \exp(\mathrm{i}\pi/3)$. The constraint (2.3) that α be a unit norm lattice vector has the solutions $\alpha = \pm 1$, $\alpha = \pm\exp(\mathrm{i}\pi/3)$ and $\alpha = \pm\exp(2\mathrm{i}\pi/3)$. All obey the second constraint (2.4). The allowed shifts are: $\beta = 0, \frac{1}{2}$ for $\alpha = \pm 1$, $\beta = 0, \frac{\tau+1}{2}$ for $\alpha = \pm\tau$ and $\beta = 0, \frac{\tau}{2}$ for $\alpha = \pm(\tau - 1)$.

(e) $\tau = \frac{1}{2} + \mathrm{i}\tau_2$ with $\tau_2 > \frac{1}{2}\sqrt{3}$. Here again $\alpha = \pm 1$. The only shifts compatible with the involution constraint are $\beta = 0, (1/2)$.

Not all these involutions are independent. Involutions $\sigma(z) = \alpha\bar{z} + \beta$ which are conjugate to each other by an automorphism of the covering space, $g(z)\sigma(z)g^{-1}(z) \simeq \sigma'(z)$ with $g(z) = az + b$, $a \in \mathbb{C}^*$ and $b \in \mathbb{C}$, have *identical* action on the torus. For such an automorphism $g(z)$ to take the period parallelogram associated with Λ into another, it must be area-preserving. Thus b is arbitrary, while a must be a square root of 1 in cases (a), (c) and (e), a fourth root of 1 in case (b) and a sixth root of 1 in case (d). Explicitly, we have therefore

$$\sigma'(z) = \alpha a^2 \overline{z} + a\beta + (b - \alpha a^2 \overline{b}), \tag{2.5}$$

since $(a/\overline{a}) = a^2$. Note also that if $\alpha a^2 = 1$ then $b - \alpha a^2 \overline{b} = 2\mathrm{i}\mathrm{Im}(b)$, whereas if $\alpha a^2 = -1$ then it equals $2\mathrm{Re}(b)$. A detailed analysis ([38] particularly Section 12.33) of each of the cases (a)–(e) above using these observations results in a complete classification of the inequivalent anti-holomorphic involutions on a torus (see table 1). To illustrate the method, let us check case (a). If $\alpha = 1$, then $\alpha a^2 = 1$, so $b - \alpha a^2 \overline{b} = 2\mathrm{i}\mathrm{Im}(b)$. We can thus choose β to be real, and since it lies in the period parallelogram, to lie in the interval $[0, 1)$. But $\overline{\beta} + \beta \in \Lambda$, so β is either 0 or 1/2. Similarly, if $\alpha = -1$, then $\alpha a^2 = -1$, so $b - \alpha a 2\overline{b} = 2\mathrm{Re}(b)$. We can thus choose β to be purely imaginary in the interval $[0, \mathrm{i}\tau_2)$. But $\overline{\beta} - \beta \in \Lambda$, so β is either 0 or $\mathrm{i}\tau_2/2$. It is noteworthy that this same classification was also found by Du Val [39] by analyzing the properties of elliptic functions on the lattices defined by these tori.

These results identify the subclass of T^2 complex structures that permit the existence of an anti-holomorphic involution.[1] This set is shown

[1] This extends the results of [41].

Table 1: Table of Anti-Holomorphic Involutions.

Case	τ	$J(\tau)$	α	β	s	Fixed pts
(a)	$\mathrm{i}\tau_2$ with$\tau_2 > 1$	$J > 1$	1	0	2	$\mathrm{Im}(z) = 0$; $\mathrm{Im}(z) = \tau_2/2$
			-1	0	2	$\mathrm{Re}(z) = 0$; $\mathrm{Re}(z)$=1/2
			1	$1/2$	0	
			-1	$\tau/2$	0	
(b)	i	1	$1 \sim -1$	0	2	$\mathrm{Im}(z) = 0$; $\mathrm{Im}(z) = 1/2$
			$\mathrm{i} \sim -\mathrm{i}$	0	1	$z = r\mathrm{e}^{\mathrm{i}\pi/4}, r \in \mathbb{R}$
			$1 \sim -1$	$1/2$	0	
(c)	$\mathrm{e}^{\mathrm{i}\theta}$ with $\pi/3 < \theta < \pi/2$	$(0,1)$	τ	0	1	$z = r\mathrm{e}^{\mathrm{i}\theta/2}, r \in \mathbb{R}$
			$-\tau$	0	1	$z = \mathrm{i}r\mathrm{e}^{\mathrm{i}\theta/2}$, $r \in \mathbb{R}$
(d)	$\mathrm{e}^{\mathrm{i}\pi/3}$	0	$1 \sim \mathrm{e}^{\mathrm{i}2\pi/3} \sim \mathrm{e}^{\mathrm{i}4\pi/3}$	0	1	$\mathrm{Im}(z) = 0, \sqrt{3}/4$
			$\mathrm{e}^{\mathrm{i}\pi/3} \sim -1 \sim \mathrm{e}^{\mathrm{i}5\pi/3}$	0	1	$\mathrm{Re}(z) = 0,\ 1/2$
(e)	$\frac{1}{2} + \mathrm{i}\tau_2$ with $\tau_2 > \frac{1}{2}\sqrt{3}$	$J < 0$	1	0	1	$\mathrm{Im}(z) = 0, \tau_2/2$
			-1	0	1	$\mathrm{Re}(z) = 0, 1/2$

in figure 2. We will see momentarily that this T^2 orientifold "moduli space" consists of two disconnected components.

To see what happens to the Kähler moduli space, we recall that the NS field $B \equiv \mathrm{Re}(\rho)$ is odd under worldsheet parity. Under an anti-holomorphic involution *combined* with worldsheet parity $B_{z\bar{z}} \to -B_{\bar{z}z}$ therefore survives. Clearly the volume is unchanged under any involution and hence the Kähler moduli space is unaffected by a type A orientifold projection (figure 2). Vice versa type A orientifolds exist for all values of ρ.

Mirror symmetry already tells us that for type B orientifolds the roles of the Kähler and complex structure moduli are reversed. One can also see directly that under a holomorphic involution all pairs of lattice vectors

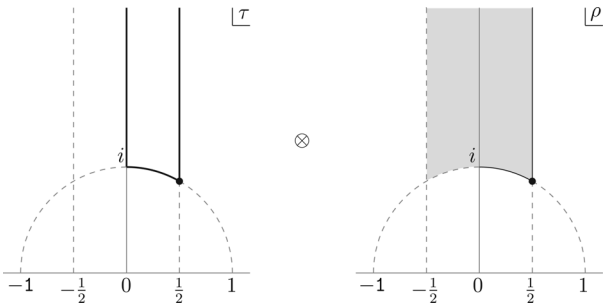

Figure 2: The "moduli space" for type A T^2 orientifolds. In figure 3, we will show that the space is not connected but there exists a topological obstruction at $\tau = i$. Type B orientifolds are related by mirror symmetry whereby the roles of τ and ρ are interchanged.

$(1, \tau)$ remain lattice vectors. To find the type B-parity compatible points in Kähler moduli space, we realize that the odd-worldsheet parity of $B_{\rm NS}$ means that under a holomorphic involution plus worldsheet parity, $\rho \to -\bar{\rho}$. Note, however, that this equation will generically bring us outside the fundamental domain (it is not defined on $\mathrm{SL}(2,\mathbb{Z})$ equivalence classes). Including an arbitrary $\mathrm{SL}(2,\mathbb{Z})$ transformation to bring us back, holomorphic involutions thus exist for Kähler moduli for which the involution returns the Kähler modulus up to an $\mathrm{SL}(2,\mathbb{Z})$ transformation, i.e., for those ρ which obey

$$-\bar{\rho} = \frac{a\rho + b}{c\rho + d}. \tag{2.6}$$

To solve this equation, recall that a convenient representation of ρ is as the ratio $\rho = \lambda_1/\lambda_2$ in terms of the components $\begin{pmatrix}\lambda_1\\ \lambda_2\end{pmatrix}$ of the fundamental representation of $\mathrm{SL}(2,\mathbb{Z})$. Equation (2.6) is therefore equivalent to the two equations

$$\begin{aligned} -\bar{\lambda_1} &= a\lambda_1 + b\lambda_2, \\ -\bar{\lambda_2} &= c\lambda_1 + d\lambda_2. \end{aligned} \tag{2.7}$$

Dividing both sides by λ_2,

$$\begin{aligned} -\frac{\bar{\lambda_2}}{\lambda_2}\frac{\lambda_1}{\lambda_2} &= a\frac{\lambda_1}{\lambda_2} + b, \\ -\frac{\bar{\lambda_2}}{\lambda_2} &= c\frac{\lambda_1}{\lambda_2} + d, \end{aligned} \tag{2.8}$$

we recognize the equations (2.3) and (2.4) with $\alpha = -\bar{\lambda_2}/\lambda_2$ (and $\beta = 0$). We therefore recover directly the inference of mirror symmetry: that the the existence of anti-holomorphic involutions in complex structure moduli-space maps to the existence of holomorphic involutions in the Kähler moduli space.

2.1.1 Fixed points, species and *O*-plane charges

It is at the fixed points of the involution that orientifold-planes are located. In the covering space $\mathbb{R}^2$ the solutions to the fixed-point equation are easily found. E.g. for anti-holomorphic involutions with zero shift they are the cycles $z\bar{z}^{-1} = \alpha$: lines through the origin at an angle $\phi = (1/2\mathrm{i})\ln(\alpha)$. Type A T^2 orientifolds therefore have $O1$-planes (we ignore the external dimensions). Fixed points of anti-holomorphic involutions are used to construct middle dimensional special Lagrangian submanifolds which can support supersymmetric D-branes. Reassuringly, this guarantees the trivial solution to the tadpole equations with D-branes on top of the O-planes.

For holomorphic involutions fixed points are even dimensional holomorphic submanifolds. For $z \to z$, the fixed submanifold is the torus itself: the O-plane is an O2-plane. For $z \to -z$, the fixed submanifold is the origin: the O-plane is an O0-plane.

The complete set of fixed points for actual T^2 involutions (a)–(e) is given in table 1. In the classification table 1 we follow Alling and Greenleaf [37, 38] in their work on Klein surfaces and real elliptic curves and attach to each non-trivial involution an invariant called the *species*, s. This is the number of connected components of the fixed point locus. In answer to one of the motivating questions, we will see this quantity re-appear on the CFT-side as the charge of the O-planes present in the Gepner construction.[2]

The geometric confirmation that the species s is related to the O-plane charge arises from the topological generating formula for O-plane charge in terms of Hirzebruch polynomials. This formula can be deduced from chiral anomaly cancellation [28, 42, 43]. In condensed notation the (set of) RR-charge(s) of an O-plane is given by

$$Q = \frac{1}{2} \int_{\text{fixed point locus}} C \wedge \sqrt{\frac{L(T/4)}{L(N/4)}}. \tag{2.9}$$

Here $C = C^{(0)} + C^{(2)} + \cdots$ denotes collectively the RR fields; $L(T)$ and $L(N)$ are the Hirzebruch polynomials of (a quarter of) the tangent and normal bundle to the O-plane localized at the fixed point. For a T^2 A-type orientifold it is a straightforward matter to show that the unique RR-charge equals the species s. Brunner and Hori showed in generality that for A-type O-planes the charge (2.9) equals half the self-intersection number of the fixed-point locus [28]. For T^2 this equals s by inspection.[3]

A closer inspection of table 1 then reveals that the species s is an obstruction in the naive "moduli space" of A-type T^2 orientifolds. The true moduli space consists of two disconnected pieces as the species number s is not arbitrary for each distinct anti-holomorphic involution. Rather involutions for $\tau = \mathrm{i}\tau_2$ only have $s = 1$, whereas involutions for which $|\tau| = 1$ or $\tau = (1/2) + \mathrm{i}\tau_2$ can only have $s = 0$ or $s = 2$. The species s therefore serves as a superselection sector on the naive "moduli space" and obstructs

[2] Alling and Greenleaf imagine the fixed point locus as the boundary of some special submanifold. Thus for them $s = 2$ corresponds to an annulus, $s = 1$ to the Möbius strip, and $s = 0$ to the Klein bottle.

[3] In general the set of all possible O-plane charges is a subset of all possible D-brane charges: one can think of the O-plane charges as a set of vectors in the D-brane charge lattice.

continuous deformation from the branch connected to large complex structure at $\tau = \mathrm{i}\infty$ to the branch connected to large complex structure at $\tau = (1/2) + \mathrm{i}\infty$. In the mirror B-0 type orientifold there are therefore two disconnected large volume T^2 orientifolds: one with the NS–NS field $B = 0$ and one with $B = 1/2$. This is directly analogous to Brunner and Hori's results on the moduli-space of the B-type orientifold of the quintic with $\tau = i$ serving as the conifold point [28]. Similar to their study we will discuss in Section 6 indications that this obstruction is lifted when the T^2 orientifold is embedded in a larger family.

2.2 The J-line moduli space

We used a natural geometric description of the moduli-space of T^2s as $\mathbb{R}^2/\Lambda$. For compactifications of phenomenological interest — Calabi–Yau orientifolds — an intrinsic geometric description of the moduli space is lacking. Rather, we only understand the complex structure moduli space in terms of deformations of algebraic equations, and the Kähler moduli space through the complex structure of the mirror. We can connect the results for T^2 compactifications with this algebro-geometric description of the moduli space through the J-function: the 1-1 map of the fundamental domain of $\mathrm{PSL}(2,\mathbb{Z})$ to the complex plane:

$$J(\tau) = \frac{2^8}{24^3} \frac{(\theta_2^8(\tau) + \theta_3^8(\tau) + \theta_4^8(\tau))^3}{(\theta_2(\tau)\theta_3(\tau)\theta_4(\tau))^8}, \tag{2.10}$$

where the $\theta_i(\tau)$ are the Jacobi θ-functions. Not coincidentally, the type A(B) complex-structure (Kähler) orientifold-moduli space projects precisely onto the real J-line. Real values of τ manifestly admit the trivial anti-holomorphic involution $\tau \leftrightarrow \bar{\tau}$ and the 1-1 correspondence between distinct tori and values of J then almost directly implies that the real J-line parametrizes the complex analytic 2-tori admitting anti-holomorphic involutions. However, it is important to note that the real J-line is *not* the moduli space for complex analytic 2-tori with anti-holomorphic involutions. As the list of anti-holomorphic involutions (a)–(e) shows, for fixed τ (i.e., J) there are multiple possible choices for the involution, and the moduli space for each is distinct although its J-value is the same. As we show in figure 3, the true moduli space is a *double cover* of the real J-line [37, 38]. On the other hand, that the moduli space is parametrized by real values of J is significant in that it suggests that the "orientifold moduli space", as a subset of the parameter space for our family of complex 2-tori, is literally the inverse image of the real part of the J-line in parameter space.

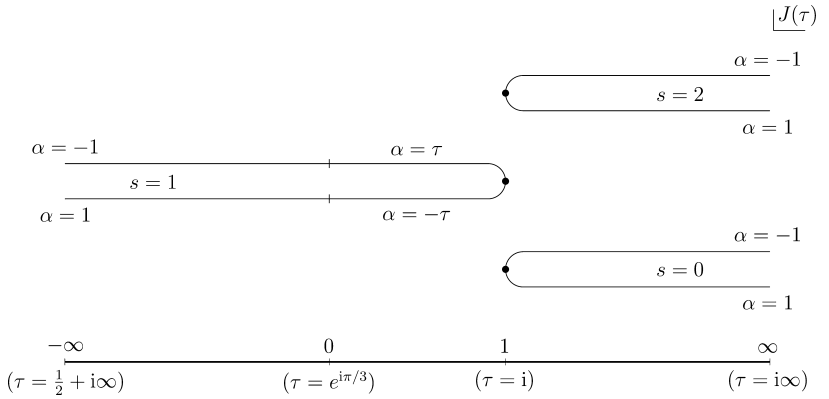

Figure 3: The complex structure (Kähler) moduli space type $A(B)T^2$ orientifolds in the $J(\tau)$-plane.

As we already indicate in figure 3, the hidden multiplicity inherent in the J-function can be resolved by two additional invariants, one of which is the species invariant s. Recall that any non-singular elliptic curve may be presented as a cubic hypersurface in *Weierstrass form* via projective coordinates $(X : Y : Z)$ where $g_2(\tau), g_3(\tau) \in \mathbb{C}$ as

$$Y^2 Z = 4X^3 - g_2 X Z^2 - g_3 Z^3, \quad \{Y, X, Z\} \sim \{\lambda Y, \lambda X, \lambda Z\}. \tag{2.11}$$

Parametrizing the $\mathbb{CP}^2$ spanned by X, Y, Z in terms of $y = Y/Z$ and $x = X/Z$, one recognizes the more conventional Weierstrass form $y^2 = W(g_2, g_3, x)$ in $\mathbb{C}^2$. In terms of the coefficients of the Weierstrass equation, the J-function — also known as the J-invariant of the elliptic curve — equals

$$J(\tau) = \frac{g_2^3}{g_2^3 - 27 g_3^2}. \tag{2.12}$$

Finite values of J correspond to a unique oriented non-singular complex elliptic curve up to isomorphism (ignoring Kähler structure).

For real elliptic curves, i.e., elliptic curves in Weierstrass form with g_2 and g_3 real, treat ∞ as a real root of $W(g_2, g_3, x)$. Then the number of real roots is 4, 2, or 0. Half this number is the species value s for the corresponding "standard" anti-holomorphic involution (i.e., the one inherited from the ambient $\mathbb{P}^2$, fixing the solutions defined over the reals).

The other invariant which, together with the species, completely determines the pair of an analytic 2-torus and an anti-holomorphic involution up to isomorphism, is essentially a square root of $J(\tau) - 1$, or rather the sign

of the discriminant [38, S17.50]:

$$\Delta = g_2^3 - 27g_3^2. \tag{2.13}$$

More precisely, consider the quartic

$$P(x) = Ax^4 + 4Bx^3 + 6Cx^3 + 4Dx + E$$

and the associated Weierstrass invariants g_2 and g_3 with $W(g_2, g_3, x) = P(x)$ (after Cayley and Boole [38, S17.30]) expressed as

$$g_2 = AE - 4BD + 3C^2, \quad g_3 = ACE + 2BCD - AD^2 - B^2E - C^3.$$

If the discriminant, Δ, is positive, then the invariant is

$$H = 3^{3/2} g_3/\sqrt{\Delta}$$

and if it is negative, then it is

$$H = 3^{3/2} g_3/\mathrm{i}\sqrt{-\Delta}$$

In either case, $H^2 = J - 1$. The function H is Huisman's "real J-invariant" [40].

2.2.1 A comparison to GLSM results for projective spaces

The Weierstrass description of the elliptic curve is, however, not a natural one from the worldsheet string. The most general description we know for string theories on Calabi–Yau surfaces is as gauged $\mathcal{N} = 2$ linear sigma models (GLSM). The target CY surface arises in algebro-geometric form from the minimum of the GLSM superpotential as the zero locus of a set of equations in weighted projective space. Brunner, Hori, Hosomichi and Walcher classified the possible anti-holomorphic involutions and their fixed point loci ([28] for unweighted and [29] for weighted projective spaces). There are three such algebraic descriptions of the torus. It is precisely these algebraic descriptions in the GLS model that make contact with the exact CFT description. At special points in the moduli space the IR limit of GLSM is given by a Gepner model. Following the Gepner notation[4] the three models are the

[4]The Gepner model $(k_1, \ldots, k_r)$ is obtained by tensoring r $\mathcal{N} = 2$ minimal models of level k_i. This corresponds to a superpotential $x_1^{k_1+2} + \cdots + x_r^{k_r+2} \in W\mathbb{P}_{H/(k_1+2),\ldots,H/(k_r+2)}$ where H is the least common multiple of the $k_i + 2$. For the variety to be Calabi–Yau the k_i must satisfy, $-1 + \sum_{i=0}^{r}(1/k_i + 2) = 0$, which might require the inclusion of trivial, $k_i = 0$, minimal models (e.g. [29, 44]).

(1,1,1) model corresponding to the variety

$$x_1^3 + x_2^3 + x_3^3 = 0, \quad x_i \in \mathbb{CP}^2 \tag{2.14}$$

which describes a torus with $\tau = \mathrm{e}^{(\mathrm{i}\pi/3)}$, the (2,2) model with variety

$$x_1^4 + x_2^4 + x_3^2 = 0, \quad x_i \in W\mathbb{CP}_{1,1,2} \tag{2.15}$$

which is a torus with $\tau = \mathrm{i}$ and the (1,4) model,

$$x_1^6 + x_2^3 + x_3^2 = 0, \quad x_i \in W\mathbb{CP}_{1,2,3} \tag{2.16}$$

which has $\tau = \mathrm{e}^{(\mathrm{i}2\pi/3)} \sim \mathrm{e}^{(\mathrm{i}\pi/3)}$.

To analyze the anti-holomorphic involutions, consider first the (1,1,1) representation of the torus as an algebraic variety in unweighted projective space: the Fermat cubic,

$$x_1^3 + x_2^3 + x_3^3 = 0, \quad x_i \in \mathbb{CP}^2. \tag{2.17}$$

The two distinct anti-holomorphic involutions are the canonical one, $x_i \mapsto \bar{x}_i$, and the permutation involution, $(x_1, x_2, x_3) \mapsto (\bar{x}_2, \bar{x}_1, \bar{x}_3)$). Following Brunner and Hori [28], we therefore expect to find two kinds of O1 planes at the fixed points corresponding to two distinct anti-holomorphic involutions. In order to make a connection to the Weierstrass description,

$$Y^2 Z = 4X^3 - g_2 X Z^2 - g_3 Z^3, \quad \{X, Y, Z\} \in \mathbb{CP}^2, \tag{2.18}$$

which allows a direct map to the lattice description through the Weierstrass functions

$$\begin{aligned} J(\tau) &= \frac{g_2^3}{g_2^3 - 27 g_3^2}, \\ X &= \wp(z;\tau) \equiv \frac{1}{z^2} + {\sum_{m,n=-\infty}^{\infty}}' \frac{1}{(z-(m\tau+n))^2} - \frac{1}{(m\tau+n)^2}, \\ Y &= \frac{d}{dz}\wp(z;\tau), \end{aligned} \tag{2.19}$$

we apply the change of variables,

$$x_1 = \frac{1}{6}Z + \frac{\sqrt{3}}{18}Y, \quad x_2 = \frac{1}{6}Z - \frac{\sqrt{3}}{18}Y, \quad x_3 = -\frac{1}{3}X. \tag{2.20}$$

This yields a Weierstrass equation with $g_2 = 0$ and $g_3 = 1$. Thus $J = 0$, which is known to correspond to $\tau = \mathrm{e}^{(\mathrm{i}\pi/3)}$. With the Weierstrass correspondence between the algebraic Fermat cubic and the lattice description in hand, we can match the anti-holomorphic involutions on both sides. For $\alpha = 1$ (and zero shift) the involution is $\tau \to \bar{\tau}$. As the Weierstrass $\wp$-function is a holomorphic function in τ with real coefficients, we see that this implies $X \to \bar{X}$ and $Y \to \bar{Y}$. The transformation to the Fermat cubic is also holomorphic and thus the involution $z \to \bar{z}$ corresponds

to the canonical involution $x_i \to \bar{x}_i$. For the involution $\tau \to -\bar{\tau}$, the definition of the $\wp$-function shows that $X \to \bar{X}$, but $Y \to -\bar{Y}$. From the transformation rules (2.20), we immediately see that this corresponds to $x_1 + x_2 \to \bar{x}_1 + \bar{x}_2$, $x_1 - x_2 \to -(\bar{x}_1 - \bar{x}_2)$ and $x_3 \to \bar{x}_3$ and hence to the permutation involution.

For an arbitrary algebraic variety in weighted projective space it was shown in [29] that the parity transformations are $x_i \to \mathrm{e}^{(\mathrm{i}2\pi m_i/k_i+2)}\bar{x}_i$, up to permutation, subject to the following equivalences: $m_i \sim m_i + 2n_i, \forall\ n_i \in \mathbb{Z}$ and $m_i \sim m_i + 1$. Thus for the (2,2) Gepner model, corresponding to a variety

$$x_1^4 + x_2^4 + x_3^2 = 0, \quad x_i \in W\mathbb{CP}_{1,1,2} \tag{2.21}$$

we expect there to be the following three types of involutions:

(1) $(x_1, x_2, x_3) \longrightarrow (\bar{x}_1, \bar{x}_2, \bar{x}_3)$,
(2) $(x_1, x_2, x_3) \longrightarrow (\bar{x}_1, \bar{x}_2, -\bar{x}_3)$,
(3) $(x_1, x_2, x_3) \longrightarrow (\bar{x}_1, \mathrm{i}\bar{x}_2, -\bar{x}_3)$.

The fixed point locus of the first case is empty, as it described by the solution set of

$$a_1^4 + a_2^4 + a_3^2 = 0, \quad a_i \in W\mathbb{RP}_{1,1,2} \tag{2.22}$$

which, as a sum of positive terms, cannot be equal to zero. According to our classification, this corresponds to a species $s = 0$ type involution (see table 1). The second case reduces to the requirement that

$$a_1^4 + a_2^4 = a_3^2, \quad a_i \in W\mathbb{RP}_{1,1,2}, \tag{2.23}$$

which appears as closed curves in the a_1, a_2 plane with a_1 intercept parametrized by $\sqrt{|a_3|}$. There are actually two disconnected curves as a_3 and $-a_3$ yield the same radius parameter. This corresponds to the double fixed point locus in our table, i.e., an $s = 2$ type involution.

The third possibility reduces to

$$a_1^4 - a_2^4 = a_3^2, \quad a_i \in W\mathbb{RP}_{1,1,2}, \tag{2.24}$$

which resembles a hyperboloid with two disconnected branches. However, a careful study of the locus, chart by chart, reveals that the two branches connect through infinity. For example, in the $a_2 \neq 0$ chart one gets the expression

$$\left(\frac{a_1}{a_2}\right)^4 - 1 = \left(\frac{a_3}{a_2}\right)^2, \tag{2.25}$$

which has two branches which intersect the $\frac{a_3}{a_1}$ axis at the points, $B^{\pm}$, given by coordinates $((a_1/a_2) = \pm 1, (a_3/a_2) = 0)$ (see figure 4). Although these

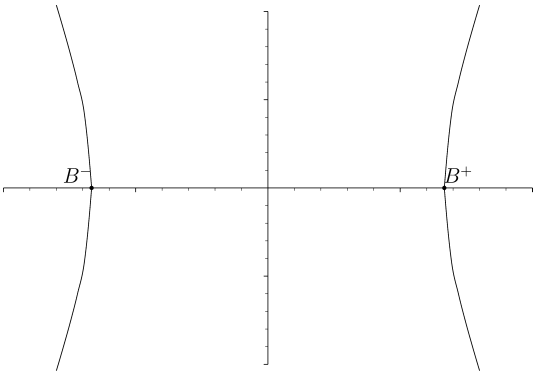

Figure 4: The curve $a_1^4 - a_2^4 = a_3^2$ in the chart where $a_2 \neq 0$.

two points appear disjoint in this chart they appear connected in the $a_1 \neq 0$ chart, where the equation reduces to

$$1 - \left(\frac{a_2}{a_1}\right)^4 = \left(\frac{a_3}{a_4}\right)^2, \tag{2.26}$$

which describes a closed loop around the origin (see figure 5). The points $B^\pm$ now appear in the opposite sides of the loop. Similarly, the chart $a_3 \neq 0$ has two apparently disconnected branches whose points are connected in the $a_1 \neq 0$ chart. Thus the third possibility has $s = 1$.

We can express the (2,2) Gepner variety in Weierstrass form,

$$ZY^2 = 4X^3 + XZ^2, \tag{2.27}$$

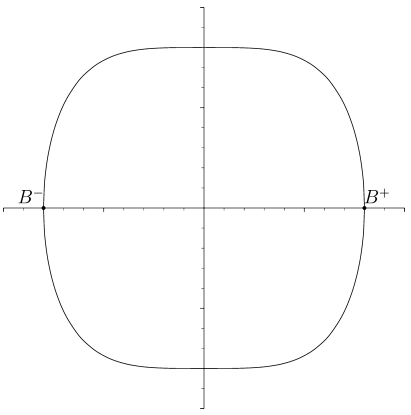

Figure 5: The curve $a_1^4 - a_2^4 = a_3^2$ in the chart where $a_1 \neq 0$.

by applying the transformations

$$x_1 = (X/Z + (1/2)), \quad x_2 = \mathrm{e}^{(\mathrm{i}\pi/4)}\,((1/2) - X/Z), \quad x_3 = \mathrm{i}Y/Z. \tag{2.28}$$

Here $J = 1$ which indeed corresponds to $\tau = \mathrm{i}$. Recall that the number of roots of the Weierstrass equation over the reals is twice the species number for the *standard* anti-holomorphic involution — i.e., just the barring of all the coordinates. With this Weierstrass form we obtain two roots $(X = 0, X = \infty)$, hence $s = 1$. Conjugating the Weierstrass variables induces the transformation

$$x_1 \longrightarrow \bar{x}_1, \quad x_2 \longrightarrow \mathrm{i}\bar{x}_2, \quad x_3 \longrightarrow -\bar{x}_3, \tag{2.29}$$

which is the third involution case we examined and showed to be of type $s = 1$.

Finally, the (1,4) model corresponds to the superpotential

$$x_1^6 + x_2^3 + x_3^2 = 0, \quad \in W\mathbb{CP}_{1,2,3}, \tag{2.30}$$

which, using the parities described in [29], has the following possible parity involutions:

(1) $(x_1, x_2, x_3) \longrightarrow (\bar{x}_1, \bar{x}_2, \bar{x}_3)$,
(2) $(x_1, x_2, x_3) \longrightarrow (\bar{x}_1, \mathrm{e}^{(\mathrm{i}2\pi/3)}\bar{x}_2, \bar{x}_3)$,
(3) $(x_1, x_2, x_3) \longrightarrow (\mathrm{e}^{(\mathrm{i}\pi/3)}\bar{x}_1, \bar{x}_2, \bar{x}_3)$,
(4) $(x_1, x_2, x_3) \longrightarrow (\bar{x}_1, \bar{x}_2, -\bar{x}_3) \ \sim (\mathrm{e}^{(\mathrm{i}\pi/3)}\bar{x}_1, \mathrm{e}^{(\mathrm{i}2\pi/3)}\bar{x}_2, \bar{x}_3)$.

The first and second cases have fixed point loci isomorphic to

$$a_1^6 + a_2^3 + a_3^2 = 0, \quad a_i \in W\mathbb{RP}_{1,2,3}. \tag{2.31}$$

This follows directly in case (1). The fixed point locus of transformation (2) is isomorphic to this curve under the map $a_2 \to -a_2$. The fixed point loci for these cases are of species $s = 1$. The cases (3) and (4) have fixed point loci that are isomorphic to

$$-a_1^6 + a_2^3 + a_3^2 = 0, \quad a_i \in W\mathbb{RP}_{1,2,3} \tag{2.32}$$

and hence are also of species $s = 1$. The isomorphism relating case (3) to case (4) is also the map $a_2 \to -a_2$. It is easier to see this if one uses the second presentation of the involution map for case (4). Thus in all there are only two different classes of involution for this non-linear sigma model, both of which have $s = 1$. This fits in nicely with our results of table 1. As a

final check, we can apply the transformation $x_1 = \lambda,\ x_2 = -\lambda^2 4^{1/3} X/Z$, $x_3 = \lambda^3 Y/Z$, to bring the elliptic curve to Weierstrass form

$$Y^2 Z = 4X^3 - Z^3. \tag{2.33}$$

We can see that the Weierstrass equation has two real roots at $X = \infty$ and at $X = (1/3)^{(1/3)}$ so that the natural involution also has $s = 1$, as was to be expected. Note that the Weierstrass equation has $J = 0$. Hence this is the same elliptic curve as the (1,1,1) model even though the value $g_3 = 1$ is different.

The importance of the species s in the analysis of involutions of T^2 and their fixed points is self-evident. We will now show how the species s appears as the O-plane charge from a microscopic worldsheet CFT analysis. We have clearly seen, however, how much an analysis solely based on geometrical methods is able to tell us.

3 Crosscaps in Calabi–Yau compactifications: review

We will use the equivalence of O-planes and worldsheet crosscaps to gain an understanding of charges and tensions of orientifold planes. First we will write down rational worldsheet CFTs which correspond to toroidal compactifications. In particular, we will work with the so called "Gepner" model of the torus. The orientifold(-planes) will then correspond to crosscaps in the CFT. This section reviews how to construct unoriented RCFTS and how to read off the O-plane data from the crosscap states. The knowledgeable reader may skip to Section 4 where we apply these methods to T^2 compactifications as $c = 3$ Gepner models.

3.1 Gepner models: a brief review

A Gepner model is a $c = 3n$, $\mathcal{N} = 2$ CFT produced by tensoring several $c_i = 3k_i/(k_i + 2)$ $\mathcal{N} = 2$ minimal models and aligning the worldsheet supersymmetry currents. The resulting $\mathcal{N} = 2$ theory, $\mathcal{A}^{3n}$, can be matched to a specific $d = 2n$ algebraic variety. The full theory requires the inclusion of the external $d = 10 - 2n$ dimensional spacetime which is modeled (via the bosonic string map [34, 45–48]) as a $\mathcal{N} = 2$ WZW $D_{N-1,1}$ component to be tensored with $\mathcal{A}^{3n}$ and again susy aligned. The resulting theory $\mathcal{A}^{ws}$ is finally GSO projected to produce a consistent string compactification.[5]

[5]When studying closed oriented theories, a pre-GSO projection can be done on the $\mathcal{A}^{3n}$ theory to produce a more or less independent CFT theory corresponding to the

Table 2: Simple currents of $\mathcal{N}=2$ minimal models. Recall that primary fields are labeled by (ℓ, m, s) with $0 \leq \ell \leq k$, $-k-1 \leq m_{\text{mod 2k+4}} \leq k+1$, $-1 \leq s_{\text{mod 4}} \leq 2$ subject to field identification $(\ell, m, s) \simeq (k-\ell, m+k+2, s+2)$ (For a review see [34, 52]).

Current	Primary field label	Order
v	(0,0,2)	2
s	(0,1,1)	$2k+4$ if $k \in 2\mathbb{Z}$, $4k+8$ otherwise
$p = s^2 v$	(0,2,0)	$k+2$
f	$(k,0,0) = (0,k+2,2)$	2

The supersymmetry alignment of the different components is an example of *a simple current extension* of a CFT. A simple current extension is an extension of the chiral algebra $\mathcal{A} \overset{J}{\subset} \mathcal{A}^{\text{ext}}$ by integer conformal weight simple currents: primary fields J whose fusion with any other primary field, i, yields a *single* field $j = Ji$ [50, 51]. Under this extension primary fields arrange themselves into orbits $[i] = \{i, Ji, J^2 i, \ldots\}$. The conformal weight of the orbit is well-defined modulo integers. The exact conformal weight of the orbit is taken to be the lowest of the weights of its representative elements [49]. Orbits with integer monodromy charge $Q_J(i) \equiv h_i + h_J - h_{Ji} \bmod \mathbb{Z}$ under J, are the primaries of the extended chiral algebra $\mathcal{A}^{\text{ext}}$. Non-integer charged fields are projected out.

The simple currents of an $c_i = 3k_i/(k_i+2)$ $\mathcal{N}=2$ minimal model are reproduced in table 2 [52]. Worldsheet supersymmetry is generated by the "vector" simple current, v_i, of order 2. The alignment of the worldsheet supersymmetries in a tensor product of $i = 1, 2, 3, \ldots, r$ minimal models is thus enforced by the group of currents generated by w_{ij}: the pairwise choice of v_i's. In our calculations, we will prefer to work in two stages. First, we will align the minimal model tensor product(the "Gepner" part, $\mathcal{A}^{3n}$) and then align it with the spacetime part $D_{8-n,1}$ to yield the worldsheet theory, $\mathcal{A}^{\text{ws}}$.

The final step in constructing the Gepner model is to perform the GSO projection which will ensure spacetime supersymmetry. This is done by extending the theory by the spectral flow operator of $\mathcal{A}^{ws}$, s, which is the product of the spectral flow operators of the individual $\mathcal{N}=2$ factors in the tensor theory. The order of the group generated by this theory depends on

internal compactification space [34]. However, in unoriented closed/open theories, the supersymmetric properties of the theory in general and crosscap states in particular cannot be divorced from the ambient space [26, 49, 27].

the structure of the components. The relevant feature is that this current is even, as described in [49].

In constructing simple current extensions there is an important subtlety that one must be aware of. When the order of the current is even, there may exist fixed points, i.e., fields $i = Ji$ that are invariant under the action of the extension current J. In general, one must resolve this degeneracy for a complete description of the theory [50, 51, 53]. However, the conjecture is that the one known consistent solution for the crosscap coefficients (see below) of orientifolded simple current extensions needs only the trivial solution to the fixed point resolution [15, 53] and we can therefore ignore this subtlety.

3.2 Building consistent $\mathcal{N} = 2$ unoriented CFTs

The worldsheet supersymmetry alignment ensures that the Gepner model will be $\mathcal{N} = 2$ superconformal. The bulk worldsheet theory symmetry currents will therefore contain a left- and right-moving copy of the $\mathcal{N} = 2$ superconformal algebra [44]

$$\begin{aligned}
[L_n, L_m] &= (n-m)L_{n+m} + \frac{c}{12}(n^3 - n)\delta_{n+m}, \\
\{G_r^{\pm}, G_s^{\mp}\} &= 2L_{r+s} \pm (r-s)J_{r+s}\frac{c}{3}\left(r^2 - \frac{1}{4}\right)\delta_{r+s}, \\
\{G_r^{\pm}, G_s^{\pm}\} &= 0, \\
[L_n, G_r^{\pm}] &= \left(\frac{n}{2} - r\right)G_{n+r}^{\pm}, \\
[J_n, J_m] &= \frac{c}{3}n\delta_{n+m}, \\
[L_n, J_m] &= -mJ_{n+m}, \\
[J_n, G_r^{\pm}] &= \pm G_{n+r}^{\pm}.
\end{aligned} \tag{3.1}$$

Important for us are the $\mathbb{Z}_2 \times U(1)$ *automorphisms* of the $\mathcal{N} = 2$ superconformal algebra. The $U(1)$ is an inner automorphism produced by conjugation with the $U(1)$ R-charge, while the $\mathbb{Z}_2$ is an outer automorphism which flips the sign of the R-charge.

These automorphisms, and in particular the involutive ones, play a constitutive part in the method of *open descendants*: the construction of consistent unoriented closed/open string theories from a consistent, i.e., modular invariant closed string theory [54–56]. Starting from the torus partition function, $\mathcal{Z}^{\text{orient}} = Z$, of this oriented closed string theory one can project, or in a sense "orbifold", by the world sheet parity operator, Ω. The resulting partition function, $\mathcal{Z} = (Z + K)/2$, is the sum of the torus contribution and

an unoriented component, K, the Klein bottle partition. The Klein bottle can be described as a tube ending on two crosscaps. Depending on how time is oriented, there are two ways of describing the physics: the "open loop channel", or the "transverse closed string channel". In the open loop, time runs azimuthally with open strings spanning the length of the tube and ending on the crosscaps. The resulting boundary condition on an open string ending on the crosscap is $\partial_\tau X(\sigma,\tau) = -\partial_\tau X(\pi/2-\sigma,\tau)$. The open string partition function can, by a conformal map aligning time with the cylinder axis, also be seen as a tree level closed string exchange between the two crosscaps. The open string boundary condition is then reinterpreted as a gluing condition at the crosscap state, $|C\rangle$,

$$W_n - (-1)^{h_W+n} w[\tilde{W}_n]|C\rangle = 0, \tag{3.2}$$

where W_n is the mode expansion of a chiral field W of weight h_W [15]. For the standard bosonic string W_n would be a string oscillator mode, α_n, and the weight would be unity. The symbol w is used to denote any possible automorphisms of the chiral algebra which could provide additional ways of matching the right and left moving algebras.

Generically the projected theory, $\tilde{\mathcal{Z}} = (Z+K)/2$, suffers from UV divergences. These can be canceled by adding new "twisted states". These come from the open string sector, described by the Annulus partition function, A, which is also in turn projected by Ω. This projection yields the sum of the Annulus and the Möbius partition functions: $(A+M)/2$. The annulus can be described as the familiar open cylinder, while the Möbius can be envisioned as a cylinder with a boundary on one end and a crosscap on the other. In the direct channel picture, we can attach an open string to the boundary so that it satisfies Dirichlet, $\partial_\tau X = 0$, or Neumann, $\partial_\sigma X = 0$, boundary conditions. In the closed string transverse channel, this boundary condition can be interpreted as the tree level exchange of closed strings from a boundary state, $|B\rangle$, with the boundary gluing condition

$$W_n - (-1)^{h_W} w[\tilde{W}_n]|B\rangle = 0. \tag{3.3}$$

For the standard bosonic string, w is the identity in the Neumann case, or the map $\tilde{\alpha}_n \to -\tilde{\alpha}_n$ in the Dirichlet case.

Formally the boundary and crosscap states can be expanded as linear combinations of boundary, $|I\rangle\rangle_{B,w}$, and crosscap, $|I\rangle\rangle_{C,W}$, Ishibashi states [57]. These Ishibashi state are solutions to the reflection conditions (3.2) and (3.3) that are (irreducible) representations of the conformal symmetry.

In this formal sense, the boundary and crosscap states are

$$|B_a\rangle_w = \sum_I B_{aI}|I\rangle\rangle_{B,w},$$
$$|C\rangle_w = \sum_I \Gamma_I|I\rangle\rangle_{C,w}. \tag{3.4}$$

Here the boundary state acquires a boundary label, a, to distinguish different boundaries. Explicitly, the boundary Ishibashi states are given by [15]

$$|I\rangle\rangle_{B,w} = \sum_s |s, I\rangle \otimes UV_w|s, I\rangle, \tag{3.5}$$

where I is a primary field of the theory and s labels the states in that module. The operator U is antiunitary and satisfies the commutation relation

$$U\tilde{W}_n = \tilde{W}_n U(-1)^{h_W}, \tag{3.6}$$

while V_w is an "intertwiner" which maps a module I to a module $w(I)$ and satisfies the composition rule

$$V_w \circ W_n = w[W_n] \circ V_w. \tag{3.7}$$

The crosscap reflection condition (3.2) is similarly solved by the crosscap Ishibashi states,

$$|I\rangle\rangle_{C,w} = \sum_s |s, I\rangle \otimes (-1)^{\tilde{L}_0 - h_I} UV_w|s, I\rangle. \tag{3.8}$$

The boundary coefficients, B_{aI}, and the crosscap coefficients, Γ_I, must obey certain "sewing" constraints for consistency of the theory. These sewing constraints are very difficult to solve in general. In practice one limits one's attention to a subset of these: the positivity and integrality constraints. Recall that the 1-loop open string partition contains information about the spectrum of the theory. Therefore the coefficients of the characters, transformed back from the transverse channel, have to be natural numbers. These conditions are already so restrictive that only one set of solutions is known. For the boundary coefficients with trivial automorphism action one has the Cardy solution [58],

$$B_{Ia} = \frac{S_{Ia}}{\sqrt{S_{I0}}}, \tag{3.9}$$

where S is the representation of the modular generator, $\tau \to -1/\tau$, on the conformal characters (irreducible building blocks of the partition function).

For the crosscap coefficients (again with trivial automorphism action) there is the Rome solution [59, 55],

$$\Gamma_I = \frac{P_{I0}}{\sqrt{S_{I0}}}, \tag{3.10}$$

where $P = \sqrt{T}ST^2S\sqrt{T}$ and T is the other generator of the modular group $\tau \to \tau + 1$.

These equations can be generalized to the case of simple current extensions [15, 49]. For a theory whose algebra, $\mathcal{A}^{\text{ext}}$, is extended from $\mathcal{A}$ by a simple current group G of order N, the boundary states are [60, 61],

$$\begin{aligned} |B_{[a]}\rangle &= \frac{1}{\sqrt{N}} \sum_{J\in G} |B_{Ja}\rangle \\ &= \sum_I \sqrt{N} \frac{S_{Ia}}{\sqrt{S_{I0}}} |I\rangle\rangle_D, \end{aligned} \tag{3.11}$$

where one uses the familiar S-matrix identity,

$$S_{Ji,j} = \mathrm{e}^{\mathrm{i}2\pi Q_J(j)} S_{i,j}, \tag{3.12}$$

and that $Q_J(I) = 0$, i.e., the Ishibashi states are labeled by "fields" I of $\mathcal{A}$ that are integer charged under J. The crosscap is similarly extended as [62]:

$$|C\rangle_\sigma^{[K]} = \sum_{J\in G} \sigma(JK) \frac{P^{\mathcal{A}}_{KJ,I}}{\sqrt{S^{\mathcal{A}}_{0,I}}} |I\rangle\rangle_C. \tag{3.13}$$

The symbols $\sigma(JK)$ are signs, where $\sigma(K) = 1$ by convention, subject to the following constraint [15]. Define $\beta_K(J) = \sigma(JK)\epsilon_J(K)$, then $\beta_K(J_1J_2) = \beta_K(J_1)\beta_K(J_2)$ and $\beta_K(0) = 1$. These constraints, valid for integer spin extensions, are equivalent to the assumption that the crosscap should only couple to fields which are GSO invariant (hence physical). The field K is a simple current in G, called the Klein bottle current; it must obey that for each order 2 current $J_2 \in G$, $Q_{J_2}(K) = 0 \mod 1$ in order to be able to solve the sign constraints. Note that K serves to label different crosscap states. The total number of boundary and crosscap states for a cyclic, $\mathbb{Z}_N$, simple current extension is therefore N boundary states and $2 \cdot N/2$ (signs times number of Klein bottles) in both cases [49]. Experience indicates that for K odd and not in G we get different crosscaps [15]. The current extensions will play an important role here in that they will be used to generate the non-trivial boundary and crosscap coefficients in addition to constructing the Gepner model.

3.2.1 Boundary conditions

Boundary and crosscap states clearly intertwine the left and right moving algebras. In particular, the full $\mathcal{N} = (2, 2)$ supersymmetry will be broken to a linear $\mathcal{N} = 2$ combination of the left and right supersymmetry algebras. The different ways a boundary or crosscap state can preserve the $\mathcal{N} = 2$ susy is thus given by the automorphisms of the $\mathcal{N} = 2$ algebra. At the same time, we wish to preserve $T|B\rangle = \bar{T}|B\rangle$ as the conserved charge associated with the unbroken translations is (worldsheet) "energy" rather than momentum; hence there is no energy leakage across the boundary. The full $U(1) \times \mathbb{Z}_2$ isomorphisms leave T unchanged and can therefore be used to vary the gluing conditions. The most general boundary conditions fall in two classes, A and B distinguished by whether the $\mathbb{Z}_2$ acts trivially (type A) or not (type B).

$$\begin{aligned} A\text{−type}: \quad & G^{\pm}|B\rangle = \mathrm{e}^{\pm \mathrm{i}\alpha_A}\bar{G}^{\mp}|B\rangle, \\ & J|B\rangle = \bar{J}|B\rangle. \\ B\text{−type}: \quad & G^{\pm}|B\rangle = \mathrm{e}^{\pm \mathrm{i}\alpha_B}\bar{G}^{\pm}|B\rangle, \\ & J|B\rangle = -\bar{J}|B\rangle. \end{aligned} \tag{3.14}$$

Note that the A-type boundary conditions preserve the $U(1)_A \equiv U(1)_{R,L} - U(1)_{R,R}$ symmetry, but break the $U(1)_V \equiv U(1)_{R,L} + U(1)_{R,R}$ symmetry, whereas the B-type boundary conditions do the reverse. There must therefore be a $U(1)_V$ *multiplet* of consistent A-type boundary conditions, and it is not hard to see that these are precisely the boundary conditions parametrized by α_A. One obtains these by a rotation by $\mathrm{e}^{\mathrm{i}(\alpha_A/2)J_V}$:

$$\begin{aligned} |B\rangle_{\alpha_A} = \mathrm{e}^{\mathrm{i}\frac{\alpha_A}{2}J_V}|B\rangle_0: \quad G^{\pm}|B\rangle_{\alpha_A} &= G^{\pm}\mathrm{e}^{\mathrm{i}\frac{\alpha_A}{2}J_V}|B\rangle_0 \\ &= \mathrm{e}^{\pm \mathrm{i}\alpha_A}\bar{G}^{\mp}|B\rangle_{\alpha_A}. \end{aligned} \tag{3.15}$$

Similarly, B-branes fall a $U(1)_A$ multiplet of boundary states, which preserve half the supersymmetry.[6] We will only consider the $\alpha_A = 0$ and $\alpha_B = 0$ representatives.

The known consistent solutions to crosscap and boundary gluing conditions are valid only for the trivial outer automorphism case (type A). However type B is mirror to type A, as it is obtained by flipping the $U(1)$ R-charges. The mirror map can be constructed as a permutation extension

[6] This is correct for superconformal theories. For a generic $N = 2$ susy theory, however, $U(1)_A$ is broken at the quantum level. It is only preserved if $c_1(\mathcal{M}_{\text{target space}}) = 0$, which is always the case for superconformal theories. (In case $U(1)_A$ is broken, the symmetry can be "restored", however, by a shift in the B_{NS}-field [28]. There is therefore exactly one B-boundary state for each value of B_{NS}. The "faulty" B-states do exist, but they do not preserve half of worldsheet susy.)

of the theory, as described in Appendix C. Hence we can obtain the type-B crosscap and boundary states as simple current extended states of the mirror type A theory [63].

3.2.2 Crosscap states

Similarly to boundary states, crosscap states will preserve some diagonal combination of the left and right $\mathcal{N} = 2$ symmetries. The procedure to build the orientifold theory is to mod out by worldsheet parity and any other involutive global symmetry, R. We insist on involutive global symmetries as we wish to preserve the geometry of the target manifold. This is important to be able to classify the theories consistently. Otherwise, one could argue that the resulting theory is just the orientifold of some orbifold of the target manifold.

Similarly to the boundary states there are two possible crosscap conditions [30],

$$\begin{aligned} A-\text{type}: \quad & G^{\pm}|C\rangle = \mathrm{e}^{\pm i\beta_A}\bar{G}^{\mp}|C\rangle, \\ & J|C\rangle = \bar{J}|C\rangle. \\ B-\text{type}: \quad & G^{\pm}|C\rangle = \mathrm{e}^{\pm i\beta_B}\bar{G}^{\pm}|C\rangle, \\ & J|C\rangle = -\bar{J}|C\rangle. \end{aligned} \tag{3.16}$$

The phases $\beta_{A,B}$ are related to the $U(1)$-automorphism class. In equation (3.21), we shall see that this determines the spacetime susy properties of the O-plane. As also in the case of boundary states, the crosscaps for the trivial automorphism class can be directly constructed, but B-type crosscaps will be obtained via the mirror simple current map from the A-type states.

3.3 Orientifolds in Gepner models

In Gepner models, an important additional step in the construction of supersymmetric BPS like crosscap states is the GSO projection. Previous studies indicated that it was possible to decouple the internal geometry of the theory from the spacetime via a "pre-GSO" projection (see e.g. [34]). However, in the context of orientifolds this separation of the theory into spacetime and internal sectors is very awkward, as without the complete GSO projection the resulting crosscaps did not satisfy the BPS condition [26, 27, 49]. Hence, a careful study of the GSO projection is necessary. Specifically the GSO projection involves the simple current extension from the worldsheet supersymmetric theory, $\mathcal{A}^{\mathrm{ws}}$, to the spacetime supersymmetry theory, $\mathcal{A}^{\mathrm{ext}}$.

This extension is generated by the spectral flow field, S, which is of even order, N_S. As described in [49], by requiring that the crosscap only couples to fields, $i \in \mathcal{A}^{\text{ext}}$, i.e., such that $Q_S(i) = 0$, the resulting A-type crosscap has the following general description:

$$|\Gamma\rangle^{\sigma}_{[K]} = \sqrt{N_S} \sum_{\{i|REP_{[i]},\ Q_S(i)=0\}} \left(\frac{\sigma_0 P_{i,K} + \sigma_1 P_{i,KS}}{2\sqrt{S_{0i}}} \right) |[i]\rangle\rangle_{\epsilon_S(K)\sigma}, \quad (3.17)$$

where σ_0, σ_1 and $\sigma = \sigma_0/\sigma_1$ are signs and

$$|[i]\rangle\rangle_{\epsilon_S(K)\sigma} = \sum_{n=0}^{N-1} [\epsilon_S(K)\sigma]^n \epsilon_{S^n}(i), |S^n i\rangle\rangle_{1,C}, \quad (3.18)$$

is the relation between Ishibashi states in $\mathcal{A}^{\text{ext}}$ and in $\mathcal{A}^{\text{ws}}$ (which in turn are the sum of Ishibashi states in the minimal model). The Klein bottle currents are required to have monodromy

$$Q_S(K) = \frac{2p}{N_S}, \quad p \in \mathbb{Z}. \quad (3.19)$$

The weights in this last sum are just phase factors,

$$\epsilon_S(i) \equiv \mathrm{e}^{\pi \mathrm{i}(h_i - h_{Si})}. \quad (3.20)$$

Therefore, the crosscap states obey a twisted gluing condition,

$$[S_n - (-1)^{n+h_S} \epsilon^*_S(K)\sigma \bar{S}_{-n}]|C\rangle^{\sigma}_{[K]} = 0. \quad (3.21)$$

The term $\epsilon^*_J(K)\sigma = (\epsilon_J(K)\sigma)^{-1}$ is the automorphism type of the state. From the monodromy restriction of K, one can see that $(\epsilon_S(K)\sigma)^{N_S} = 1$, so that the automorphism type of the plane takes values in $\mathbb{Z}_{N_S}$. This gluing condition implies that the planes preserve the supersymmetry generated by the linear combination $S_0 + \epsilon^*_S(K)\bar{S}_0$ [49]. As S_0 generates a discrete $\mathbb{Z}_{2N_S}$ subgroup of the $U(1)_R$ symmetry, we recognize that ϵ^*_S determines the phase β_A from the previous subsection.

3.4 Crosscap and boundary mass and charges

By considering the overlap with different massless fields, we can get the tensions and charges of the boundary or crosscap state. These charges encode geometric characteristics of the corresponding orientifold or D-brane. The overlap with the massless NS–NS vacuum state, $[[\vec{0}; \vec{0}; \vec{0}]o_D]$, is proportional

to the tension of these states.[7] It is convenient to also compute the boundary state data, as at the end of the day one has to make sure that the D-brane tadpole divergences are canceled by O-plane charges.

From the crosscap expansion equation (3.17), we see that the tension is

$$M_C^{[K]} = \langle O|C\rangle^{\sigma}_{[K]} = \sigma_0 \frac{\sqrt{N_S}}{2\sqrt{S_{O,O}}} P^{\rm ws}_{O,K}, \tag{3.22}$$

where the prefactor is just a Gepner model dependent overall normalization. In the case of the boundary state, the overlap of the boundary state, (3.11), with the vacuum gives a mass of

$$M_B^{[a]} = \langle O|B_{[a]}\rangle = \sqrt{N S^{\rm ws}_{0a}}. \tag{3.23}$$

The other characteristics to determine are the charges with respect to RR ground states. In the non-linear sigma-model realization of the theory, the RR ground states of left and right $U(1)_R$charge, $(q, \tilde{q})$ can be identified with holomorphic $(n/2 - q, n/2 + \tilde{q})$ forms [29].[8] One could directly get the charges by computing the overlap of the crosscap or boundary state with the RR groundstate corresponding to primary field, $i_{RR_{gs}}$,

$$\begin{aligned} Q_i^{\rm crosscap} &= \langle i_{RR_{\rm gs}}|C\rangle = \Gamma_{i_{RR_{\rm gs}}}, \\ Q_i^{{\rm brane},a} &= \langle i_{RR_{\rm gs}}|B_a\rangle = B_{a i_{RR_{\rm gs}}}. \end{aligned} \tag{3.24}$$

However, the RR ground states are in one to one correspondence with the NS–NS chiral–chiral or chiral–antichiral primaries by spectral flow [44, 64], and it is more convenient to use chiral–antichiral fields to compute the charges. In a minimal model of level k_i chirals (antichirals) are labeled by $\chi_{\pm l_i} = (l_i, \pm l_i, 0)$, $l_i \in \{0, \ldots, k_i\}$, have charge $q_i = (\pm l_i/k_i + 2)$ and weight $h_i = |q_i|/2$. In constructing a Gepner model chiral we can take the tensor of minimal model chirals as long as they satisfy the GSO projection, $Q_S(\chi) = \sum_{i=1}^{r}(l_i/2(k_i+2)) + Q_{s_D}(f_D) = 0 \mod 1$, where the contribution for the (chiral) spacetime fields is $Q_{s_D}(v_D) = 1/2$ or $Q_{s_D}(o_D) = 0$.

A chiral–chiral primary, i, of charge $(q, \tilde{q} = q)$ corresponds, by symmetric left–right spectral flow, to a harmonic forms $(n - q, q)$ in the horizontal

[7] The fields are labeled according to tensor components: $[[\vec{l}; \vec{m}; \vec{s}]f_D] = [[l_1 \cdots l_r; m_1 \cdots m_r; s_1 \cdots s_r]f_D]$, for a tensor product of r minimal models and a $D_{8-n,1}$ spacetime component whose fields f_D are either scalar (o_D), spinor (s_D), vector (v_D) or conjugate spinor (c_D). The square brackets indicate that it is an equivalence class of fields under the simple current extension. Further details on notation can be found in the appendices. In addition, [49] contains a short review on the properties of the spacetime algebra, $D_{8-n,1}$.

[8] Note that the R-charges/harmonic form identification here is for the internal sector of the theory, so the R-charge should be restricted to the minimal models.

cohomology. The flow is generated by S, so that $i_{RR_{\rm gs}} = Si$. As they have equal charges in the left and right moving fields they naturally couple to A-type Ishibashi states giving us the A-type charges

$$\begin{aligned} Q_i^{\rm crosscap} &= \langle i_{RR_{\rm gs}}|C\rangle = \langle Si|C\rangle \\ &= \Gamma_i = \frac{\sqrt{N_S}}{2\sqrt{S_{0i}}}\sigma_1 P_{i,K}\epsilon_S(K)\epsilon_S(i). \end{aligned} \tag{3.25}$$

Chiral–antichiral primaries of charge $(q, \tilde{q} = -q)$, correspond by asymmetric left–right spectral flow, to harmonic forms in the vertical cohomology. These states naturally couple to B-type Ishibashi states. The B-type crosscap (and boundary) states are given by a non-trivial automorphism of the susy algebra. As mentioned earlier this is the same as flipping the $U(1)$ R-charges of the right moving chiral algebra. This is equivalent to working with the conjugate modular invariant instead of the diagonal modular invariant which we have been using as a starting point for A-type states. In particular, we can construct the charge conjugate invariant partition function as a simple current (permutation) extension of the diagonal theory by the currents of the Mirror Symmetry Extension group $G_{\rm ms}$. The $G_{\rm ms}$ is the simple current description of the mirror map of Greene and Plesser generated by elements of the form

$$\begin{aligned} G_{\rm ms} = \left\{ v_D^{(n+r)\epsilon}\Pi_{r=1}^r p_i^{\alpha_i}, \sum_{i=1}^r \frac{\alpha_i}{h_i} - \frac{(n+r)\epsilon}{2} = 0 \bmod 1, \quad \epsilon \in \{0,1\} \right\} \\ \bmod G_{\rm ext} \end{aligned} \tag{3.26}$$

(details on the construction of this simple current group are given in Appendix C). We can then describe B states as $G_{\rm ms}$ and G_S extension states of the $\mathcal{A}^{\rm ws}$ theory. In effect, the B-type states end up being a weighted sum of A-type states:

$$\begin{aligned} \Gamma_i^{K,B} &= \sum_{J\in G_{\rm ms}, S^n \in G_S} \frac{1}{\sqrt{N_S N_{\rm ms} S_{oi}}}\sigma(JS^nK) P^{\rm ws}_{S^nJK,i} \\ &= \sum_{J\in G_{\rm ms}} \sigma(JK)\frac{1}{\sqrt{N_{\rm ms}}}\Gamma^{JK}, \end{aligned} \tag{3.27}$$

$$\begin{aligned} B^B_{a,i} &= \frac{1}{\sqrt{N_{\rm ms}}} \sum_{J\in G_{\rm ms}, S^n\in G_S} \sqrt{\frac{N_S}{S_{oi}}} S_{S^nJK,i}, \\ &= \sqrt{N_{\rm ms}} B_{a,i}, \end{aligned} \tag{3.28}$$

where $N_{\rm ms}$ is the order of the $G_{\rm ms}$ and $\sigma(JK)$ are signs that have to satisfy some consistency conditions:

$$\beta_{MJ} = \beta_M \beta_J e^{i2\pi X(M,J)}, \tag{3.29}$$

where

$$\beta_J = \sigma(JK)\epsilon_J(K), \tag{3.30}$$

$$\epsilon_J(K) = \mathrm{e}^{\mathrm{i}\pi(h_K - h_{JK})}, \tag{3.31}$$

$$X(J^m, J^n) = -nmh_J. \tag{3.32}$$

Since the extension current has a non-integer spin, we have had to generalize the constraints on the β's by the X matrix which encodes data for making the simple current extension [15]. Details on the X matrix and its properties are found in the appendix. The β's depend on K by the requirement that the σ's are signs. These constraints only uniquely determine the signs of $\sigma(MK)$ terms where $M = L^2$ for some L. The remaining signs provide additional degrees of freedom in constructing alternative crosscaps. The exact details of the mirror symmetry map and the required signs depend on the particular model in question, so the calculations will be done in a case by case basis. An illustrative example is presented in Appendix C.2. It is evident that the charges are then directly computable once the chiral labels and the P-matrix are known. The P-matrix for the Gepner model has been computed and is presented in Appendix B. The listing of chiral labels, although simple is tedious and model dependent. Given this information it is possible to compute the charges for any Gepner model. The goal of this paper is to examine one dimensional Calabi–Yaus–tori. The specifics of these geometries will be addressed shortly.

4 Orientifold planes from Crosscap states in $c = 3$ Gepners

4.1 A torus simplification

In our study, $c = 3$ Gepner models corresponding to T^2s, the low dimensionality of the torus results in an important simplification in the computation of the charges. Geometrically this simplification occurs because the only non-trivial complex harmonic forms are of type $h^{0,0}$, $h^{1,0}$, $h^{0,1}$ and $h^{1,1}$. These cohomology rings are in one-to-one correspondence with RR-ground states of the CFT. Spectral flow which maps the $U(1)_R$ charges as, $(q, \tilde{q}) \to (q \pm c/6, \tilde{q} \pm c/6)$ in turn relates this to the ring of (NS–NS) chiral primaries. The torus has central charge $c = 3$, so the maximum chiral charge is $q = c/3 = 1$. For the left–right symmetric theory, corresponding to A-type states, one makes the identification between the (c, c) ring, the RR-ground states and the non-trivial harmonic forms as (see e.g. [44])

$$(0,0)_{\mathrm{NSNS}} \longrightarrow (-1/2, -1/2)_{RR_{\mathrm{gs}}} \quad \Longleftrightarrow \quad h^{1,0},$$

$$(1,1)_{\mathrm{NSNS}} \longrightarrow (1/2, 1/2)_{RR_{\mathrm{gs}}} \quad \Longleftrightarrow \quad h^{0,1},$$

where the spectral flow has signs $(-,-)$. However, it is possible to identify the chiral (0,0) state with both RR ground states by applying spectral flow in the opposite direction:

$$(1/2,1/2)_{RR_{\rm gs}} \longleftarrow (0,0)_{\rm NSNS} \longrightarrow (-1/2,-1/2)_{RR_{\rm gs}}. \tag{4.1}$$

The left ground state is generated by spectral flow of $(+,+)$. Flow of type $(-,-)$ is generated by S, while the $(+,+)$ is made by the conjugate field, S^c. A representative element of $h^{1,0}$ is then given by $|S\rangle$. A direct overlap calculation using the crosscap expansion, (3.17), thus yields the dZ charge[9]

$$Q_z^{[K]} = \langle dZ|\Gamma\rangle^s_{[K]} = \frac{\sigma_1\sqrt{N_S}}{2\sqrt{S_{O,O}}}\mathrm{e}^{\mathrm{i}\pi Q_s(K)}P^{\rm ws}_{O,K}, \tag{4.2}$$

$$Q_{\bar z}^{[K]} = \langle d\bar Z|\Gamma\rangle^s_{[K]} = \frac{\sigma_1\sqrt{N_S}}{2\sqrt{S_{O,O}}}\mathrm{e}^{-\mathrm{i}\pi Q_s(K)}P^{\rm ws}_{O,K}, \tag{4.3}$$

while the second equation, corresponding to $d\bar Z$ charge, is given by the overlap with $|S^c\rangle$. Up to a phase this agrees with the expression for the tension, (3.22). This should not be surprising, as the central charge of the theory is given by the overlap with the top form (dZ for the torus), and supersymmetry equates the mass and magnitude of the central charge for BPS objects.

Using the D-brane expansion, (3.11), one can similarly get the A-type D-brane charges

$$Q_z^{\rm brane}(K) = \mathrm{e}^{2\pi\mathrm{i}Q_s(K)}\sqrt{NS^{\rm ws}_{0K}}. \tag{4.4}$$

In the case of the torus, the central charge can be easily understood geometrically. Consider a torus whose lattice is made of two vectors of length R_1 and R_2 meeting at an angle θ. This can be transformed to the standard torus lattice spanned by $\{1,\tau\}\in\mathbb{C}$, where $\tau = \mathrm{e}^{\mathrm{i}\theta}R_2/R_1$. These lattice vectors define the $\hat\alpha$ and $\hat\beta$ cycles of the torus. Integration of the holomorphic top form, $\Omega = dZ$, with respect to these cycles yields the period vector of the torus:

$$\int_{\hat\alpha}\Omega = 1, \quad \int_{\hat\beta}\Omega = \tau, \tag{4.5}$$

so that,

$$dZ = dX + \tau dY, \tag{4.6}$$

where $X, Y \in (0,1)$ describe two real axis aligned with the lattice. At low energy, the A-type states are related to special lagrangian manifolds. In the torus, these are straight line loci, which can be accordingly decomposed in terms of $\hat\alpha$ and $\hat\beta$ cycles. Correspondingly the A-type orientifold/brane in

[9] $Q_s(K)$ is usually defined mod 1, however to make sense of this definition one must use the true conformal weights of the fields.

the torus T^2 is expected to be characterized by a middle homology class $\Gamma = n\hat{\alpha} + m\hat{\beta} \in H_1(T^2, \mathbb{Z})$. This class can be described according to its charge under the RR gauge fields corresponding to the NLSM elements $\{dZ, d\bar{Z}\}$:

$$Q_z = \langle dZ|\Gamma\rangle = \int_\Gamma dZ = n + m\tau, \tag{4.7}$$

$$Q_{\bar{z}} = \langle d\bar{Z}|\Gamma\rangle = \int_\Gamma d\bar{Z} = n + m\bar{\tau}. \tag{4.8}$$

These equations can be inverted to yield the cycle content,

$$n = -\frac{\bar{\tau}Q_z - \tau Q_{\bar{z}}}{2\mathrm{i}\tau_2}, \tag{4.9}$$

$$m = \frac{Q_z - Q_{\bar{z}}}{2\mathrm{i}\tau_2}, \tag{4.10}$$

which encode the central charge.

The B-type states are built from conjugate modular invariants where the Left and Right sectors have opposite chiral charges. Anti-symmetric spectral flow of signs $(+-)$ can then be used to relate the chiral-antichiral primaries with the vertical cohomology:

$$\begin{aligned} h^{1,1} : (0,0)_{\mathrm{NSNS}} &\longrightarrow (-1/2, 1/2)_{RR_{\mathrm{gs}}}, \\ h^{0,0} : (1,-1)_{\mathrm{NSNS}} &\longrightarrow (1/2, -1/2)_{RR_{\mathrm{gs}}}. \end{aligned}$$

Like in the A-type case, one can also flow the NS–NS vacuum to the $h^{0,0}$ RR ground state by using a flow with signs $(-+)$

$$(1/2,-1/2)_{RR_{\mathrm{gs}}} \longleftarrow (0,0)_{\mathrm{NSNS}} \longrightarrow (-1/2,1/2)_{RR_{\mathrm{gs}}}. \tag{4.11}$$

Thus we see that the these charges are the result of overlap with B-type primaries, $|S\rangle_B$ and $|S^c\rangle_B$. Equation (3.27) allows us to express the B-type crosscap coefficients in terms of the A-type, so we can obtain the B-charges as combinations of the A-charges:

$$Q_z^{[K],B} = \frac{1}{\sqrt{N_{\mathrm{ms}}}} \sum_{J \in G_{\mathrm{ms}}} \sigma(J,K) Q_z^{[JK]}. \tag{4.12}$$

Similarly, one can use the Mirror Symmetry extension of the boundary states, (3.28), to get the B-type D-brane charges:

$$Q_z^{B-\mathrm{brane}}(K) = \sqrt{N_{\mathrm{ms}}} Q_z(JK). \tag{4.13}$$

We will apply these equations to the different Torus Gepner models to obtain the charges and tensions of the O-planes and, for comparison, D-branes.

4.2 The (1, 1, 1) Gepner model

The $(1,1,1)$ Gepner model consists of the product of three level $k=1$ minimal models with a $D_{7,1}$ spacetime component. The internal geometry can be described by the variety

$$x_1^3 + x_2^3 + x_3^3 = 0, \quad x_i \in \mathbb{CP}^2, \tag{4.14}$$

which corresponds to a torus with $\tau = \mathrm{e}^{(\mathrm{i}2\pi/3)} \sim \mathrm{e}^{(\mathrm{i}\pi/3)}$. The first step in constructing crosscaps is determining the set of Klein bottle currents (KBCs), K. Recall that these are simple currents in the theory $\mathcal{A}^{\mathrm{ws}}$ which satisfy, $Q_S(K) = 2p/N_S \bmod 1$, $p \in \mathbb{Z}$. The number of available KBC labels is therefore $N_S/2$, where N_S is the order of the group generated by S. However, there is a sign freedom associated to each Klein bottle label yielding a total of N_S different crosscaps. In this Gepner model $N_S = 6$ and there are three different KBCs. For simplicity, we will choose the KBCs representatives to be of the form, $K = [[\vec{0}; \vec{m}; \vec{0}]o_D]$ which will be denoted as (m_1, m_2, m_3). Each m_i is either zero or ± 2. Using the equations (4.2) and (3.22), we can construct a table of O-plane charges and tensions. In table 3, the KBC label is listed in the first column, and the corresponding tensions and charges are in the last two columns. The results in the table are all normalized by the mass of the D-branes, which is the same for all K labels. Note that the tension and charge have sign degrees of freedom, σ_0 and σ_1. One of these can be determined by the tadpole cancellation condition [15], leaving free the relative sign. The second column lists the monodromy charge of the Klein bottle current. This distinguishes different KBC orbits and is related to the automorphism class of the crosscap, $\sigma\epsilon_S(K)$ which is $\mathrm{e}^{\mathrm{i}\pi Q_S(K)}$.

For comparison, we can use equations (3.23) and (4.4) to also compute the data corresponding to boundary A-type states with boundary labels equal to the KBCs. The boundary automorphism class is given by $\mathrm{e}^{\mathrm{i}2\pi Q_S(K)}$, where $2\pi Q_S(K)$ has the nice geometric interpretation of being the angle which the boundary locus makes with the torus lattice, as shown in figure 6. Not surprisingly, this diagram is compatible with the decomposition

Table 3: Summary of results for D-branes and O-planes in (1,1,1) Gepner model. Results are normalized by M^{brane} which is the same for all K.

K	$Q_s(K)$	M^{brane}	Q_z^{brane}	$\sigma_0 M^{\mathrm{crosscap}}$	$\sigma_1 Q_z^{\mathrm{crosscap}}$
$(-2,2,2)$	$1/3$	1	τ	1	$1+\tau$
$(-2,-2,2)$	$2/3$	1	$-1-\tau$	1	τ
$(0,0,0)$	1	1	1	-1	-1
$(-2,2,0)$	1	1	1	1	1

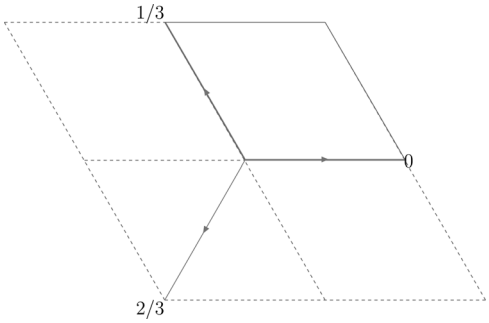

Figure 6: D-branes in $(1,1,1)$ Gepner model. The fundamental torus has solid red outline, while the D-branes cycles appear as green arrows.

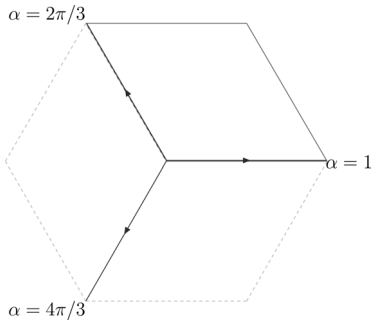

Figure 7: Diagram of O-plane loci in the $(1,1,1)$ Gepner model. The three different loci are automorphic and correspond to the same involution class, $\alpha = 1 \sim \mathrm{e}^{(\mathrm{i}2\pi/3)} \sim \mathrm{e}^{(\mathrm{i}4\pi/3)}$. The fundamental torus is outlined by solid red lines while the rotated (automorphic) ones are outlined with orange hashes.

of the underlying Special Lagrangian cycle approximation of the low energy D-brane in terms of the $\hat{\alpha}$ and $\hat{\beta}$ torus cycles (i.e., the 1 and τ coefficients in the D-brane charge). The D-brane charges are dual to these homology elements and thus form a lattice, which in this case can be seen to be generated by $\{1, \tau\}$. Although the O-planes are not expected to have a classical analogue and do not obviously add to form a homology sublattice, we can formally combine their charge vectors to span a sublattice of the D-brane charges. Examining the O-plane charges we notice that this *pro forma* charge lattice is also generated by $\{1, \tau\}$. Plotting the cycles dual to the O-plane charges yields figure 7, where it is seen that the O-plane coincides with the fixed point loci of the involution table 1. Both the D-brane and the O-plane diagram exhibit the $\mathbb{Z}_3 \subset \mathbb{Z}_6$ rotational symmetry of the $\tau = \mathrm{e}^{(\mathrm{i}\pi/3)}$ torus. The (1,1,1) Gepner model only manifestly preserves this

$\mathbb{Z}_3$ subgroup rather than the full geometric $\mathbb{Z}_6$ toroidal symmetry. This $\mathbb{Z}_3$ symmetry maps the O-planes into each other. As a result, they are all equivalent and correspond to the same involution class of table 1 given by the parameter $\alpha = 1 \sim \mathrm{e}^{(\mathrm{i}2\pi/3)} \sim \mathrm{e}^{(\mathrm{i}4\pi/3)}$. The Gepner $\mathbb{Z}_3$ symmetry generated by g acts on this involution, I_α parameter as $gI_\alpha g^{-1} = \mathrm{e}^{(\mathrm{i}2\pi/3)}\alpha$. This $\mathbb{Z}_3$ symmetry is displayed by the action on the periods:

$$\begin{aligned} 1 &\longrightarrow \tau, \\ \tau &\longrightarrow -1 - \tau. \end{aligned} \tag{4.15}$$

Note that the angle of inclination of a given O-plane is $\pi Q_S(K)$ with orientation given by the sign choice, σ_1 (i.e., a shift of the angle by π), rather than by $2\pi Q_S(K)$ as in D-branes.

In order to study B-type states we use the mirror symmetry map, described by equation (3.26), which tells us that the group responsible for the mirror map is $\mathbb{Z}_3 \times \mathbb{Z}_3$ with generators $p_1 p_2^2$ and S^2. To obtain the B-type states we only need to extend $\mathcal{A}^{\mathrm{ext}}$ by the mirror symmetry group mod GSO, i.e., by the $\mathbb{Z}_3$ group generated by $J = p_1 p_2^2$. From equation (3.27), it is apparent that one only needs to obtain the $\sigma(J, K)$ signs. This is dependent on the K label. It so happens that the signs generated by the mirror symmetry extension, $\sigma(J, K)$ conspire with the P^{ws} matrix signs to generated an overall scaling of $\sqrt{3}$ for the crosscap, which is identical to the boundary state scaling under mirror symmetry. Upon normalizing the results, we get a charge table identical to the A-type table, table 3. As expected this model is self-mirror. The mirror to $K = (-2, 2, 2)$ is calculated as an illustrative example in Appendix C.2.

4.3 The (1, 4) Gepner model

The $(1, 4)$ Gepner model corresponds to the product of a $k = 1$ and a $k = 4$ minimal model with a $D_{7,1}$ spacetime component. The presence of an even current in principle should alert us to fixed points in the simple current extensions. We explained, however, that this is not relevant for the computation of O-plane charges.

The low energy underlying geometry of this model has a representation as the solution set of

$$x_1^6 + x_2^3 + x_3^2 = 0, \quad x_i \in W\mathbb{CP}_{1,2,3}, \tag{4.16}$$

Table 4: Gepner (1,4) Model Charges and Tensions for D-branes and O-planes labeled by K and normalized by the D-brane tension, which is constant for all K.

K	$Q_S(K)$	M^{brane}	Q_z^{brane}	$\sigma_0 M^{\text{crosscap}}$	$\sigma_1 Q_z^{\text{crosscap}}$
$(2,-2)$	$1/6$	1	τ	$\sqrt{3}$	$1+\tau$
$(2,0)$	$1/3$	1	$\tau-1$	-1	$-\tau$
$(2,2)$	$1/2$	1	-1	$\sqrt{3}$	$-2\tau+1$
$(2,4)$	$2/3$	1	$-\tau$	1	$-\tau+1$
$(2,6)$	$5/6$	1	$-\tau$+1	$\sqrt{3}$	$2-\tau$
$(2,-4)$	0	1	1	1	1

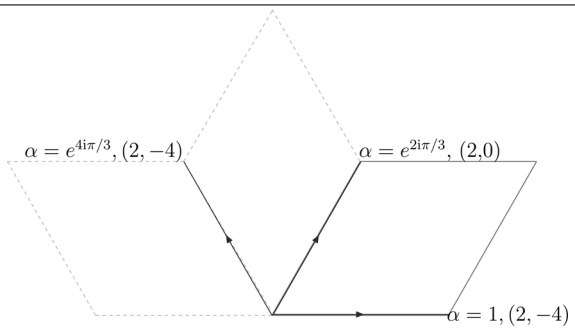

Figure 8: O-planes for (1,4) Gepner model $\alpha = 1 \sim \mathrm{e}^{(\mathrm{i}2\pi/3)} \sim \mathrm{e}^{(\mathrm{i}4\pi/3)}$ involution conjugacy. The three different labeled cycles are equivalent under the automorphism of this torus and correspond to different representative elements of the same involution conjugacy class. The Gepner symmetry on the covering plane is a rotation by $\pi/3$. This manifests itself as an ST action on the complex structure. The fundamental torus is outlined with solid red lines. Hashed orange lines are the rotated tori.

which again corresponds to a torus with $\tau = \mathrm{e}^{(\mathrm{i}\pi/3)}$. Although this torus is $\mathrm{PSL}(2,\mathbb{Z})$ equivalent to that of the $(1,1,1)$ Gepner model the symmetries of the (1,4) Gepner model are richer, spanning the full geometric $\mathbb{Z}_6$. To classify the KBCs, we note that the spectral flow group has order $N_S = 12$, so we can choose six KBCs as representatives of the possible crosscaps. As before, one can use the equations (3.22) and (4.2) to compute a table, table 4, of tensions and charges for the A-type states. The charges are normalized by the D-brane mass, which is independent of K. As in the previous case one can interpret the charges in terms of the $\hat{\alpha}$ and $\hat{\beta}$ torus cycles. When diagrammed (see figures 8 and 9) on the torus lattice, the crosscap cycles are seen to correspond to the fixed point loci listed in table 1. As emphasized, the richer Gepner symmetry, $\mathbb{Z}_6$, now allows for the two distinct involution classes listed in table 1. We can obtain all involution

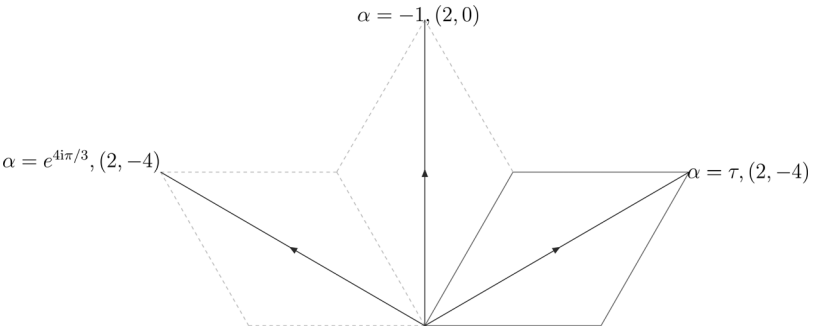

Figure 9: The (1,4) Gepner model O-planes for the $\alpha = -1 \sim \mathrm{e}^{(\mathrm{i}\pi/3)} \sim \mathrm{e}^{(\mathrm{i}5\pi/3)}$ involution conjugacy class. The three different cycles are equivalent under the automorphism of this torus. This Gepner symmetry acts as a rotation by $\pi/3$ on the covering space. This rotation manifests itself as an ST action on the complex structure. The fundamental torus is outlined with solid red lines, while the rotated (automorphic) ones are outlined with orange hashes.

classes by $g_6^n I_\alpha g_6^{-n} \to \mathrm{e}^{(\mathrm{i}n/3)}\alpha$. The O-planes transform as $\mathbb{Z}_6$ orbits whose action on the periods is

$$\begin{aligned} 1 &\longrightarrow \tau, \\ \tau &\longrightarrow \tau - 1. \end{aligned} \tag{4.17}$$

Naturally there are two separate O-plane orbits depending on the involution class. For the involution class $\alpha = 1 \sim \mathrm{e}^{(\mathrm{i}2\pi/3)} \sim \mathrm{e}^{(\mathrm{i}4\pi/3)}$ the O-planes are shown in figure 8. Those compatible with the second involution class, $\alpha = \mathrm{e}^{(\mathrm{i}\pi/3)} \sim -1 \sim \mathrm{e}^{(\mathrm{i}5\pi/3)}$ are diagrammed in figure 9. The two involution classes produce two separate charge lattices:

- $\alpha = 1 \sim \mathrm{e}^{(\mathrm{i}2\pi/3)} \sim \mathrm{e}^{(\mathrm{i}4\pi/3)}$ generated by $\{\tau + 1, 2\tau - 1\}$,
- $\alpha = \mathrm{e}^{(\mathrm{i}\pi/3)} \sim -1 \sim \mathrm{e}^{(\mathrm{i}5\pi/3)}$ generated by $\{1, \tau\}$, like the Gepner (1,1,1) Model.

Let us re-emphasize that for O-planes this charge lattice is pro forma only; see the comment above equation (4.15).

For comparison, we can repeat the analysis for A-type D-branes with boundary label K by reading of the tensions and charges from equations (3.23) and (4.4). The results for these boundary states are included in the first two columns of table 4. Figure 10 displays these D-branes as straight lines in the covering space of the torus. As expected the generators of the D-brane charge lattice are $\{1, \tau\}$.

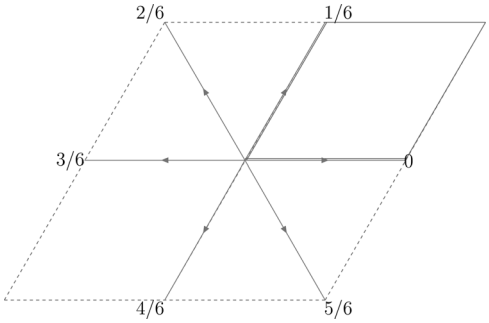

Figure 10: D-branes for the (1,4) Gepner model seen as straight lines in the covering space. Dashed delimit tori domains. Arrows mark the D-branes, which are labeled by $Q_s(K)$. The fundamental torus is outlined with solid red lines.

An other example of the richness of the symmetries of the $(1,4)$ Gepner model is that the mirror symmetry group is actually a subgroup of the GSO simple current extension group. Hence, this torus is manifestly self mirror. This is apparent from the CFT side as the GSO extended theory is self conjugate (i.e., the conjugation matrix is the diagonal). As a result the table of A-type charges and tensions (table 4) is also a valid summary for B-type states.

4.4 The (2, 2) Gepner model

The (2,2) Gepner model is generated by tensoring two level $k = 2$ Minimal models with a $D_{7,1}$ spacetime part. It has the algebro-geometric description

$$x_1^4 + x_2^4 + x_3^2 = 0, \quad x_i \in W\mathbb{CP}_{1,1,2} \tag{4.18}$$

and corresponds to a torus with $\tau = \mathrm{i}$. The GSO extension is by a group of order $N_S = 8$ so we need four Klein bottle currents. Proceeding as in the previous case we can use (3.22) and (4.2) to compile a table of charges and tensions for the crosscaps of this model (see table 5, note that the data are normalized by the D-brane mass, which is constant). Some new features arise when examining these results. First we can see that the O-planes indexed by KBC (0,0) and (0,4) have no mass nor charge. These are real states with physical interactions, as the coupling to other fields (given by other P-matrix elements) are not identically zero. They seem to correspond to orientifolds without O-planes — as these are states which have no mass or charge singularity. Interestingly enough, our involution classification for this torus, table 1, has an involution conjugacy class $\alpha = 1 \sim -1$ with $\beta = 1/2$ and $s = 0$, i.e., with no fixed points. That

Table 5: Gepner $(2,2)$ Model charges and tensions for O-planes and D-branes labeled by K. The table is normalized by the D-brane masses, which are independent of K.

K	$Q_s(K)$	M^{brane}	Q_z^{brane}	$\sigma_0 M^{\text{crosscap}}$	$\sigma_1 Q_z^{\text{crosscap}}$
$(-2,-2)$	$1/2$	1	-1	2	2τ
$(-2,2)$	0	1	1	2	2
$(-2,4)$	$1/4$	1	τ	$\sqrt{2}$	$1+\tau$
$(2,4)$	$-1/4$	1	$-\tau$	$\sqrt{2}$	$1-\tau$
$(0,0)$	0	1	1	0	0
$(0,4)$	$1/2$	1	-1	0	0

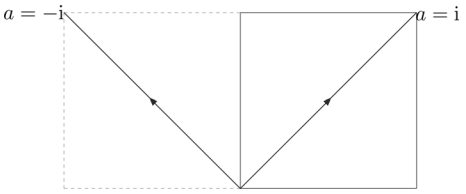

Figure 11: Gepner $(2,2)$ model O-planes seen as straight lines for the $a = \mathrm{i} \sim -\mathrm{i}$ class involution. The fundamental torus is outlined by solid red lines while the rotated automorphic one is outline by hashed orange lines.

involutions with a "shift" generate orientifolds without O-planes is in fact well known.[10]

According to the involution table there should be two more involution classes. This Gepner model manifestly has the full geometric symmetry, $\mathbb{Z}_4$, so we do expect to find O-planes corresponding to both involution classes. The action on the periods is

$$\begin{aligned} 1 &\longrightarrow \tau, \\ \tau &\longrightarrow -1. \end{aligned} \tag{4.19}$$

The $\alpha = \mathrm{i} \sim -\mathrm{i}$ involution can be seen to correspond to O-planes along the diagonal of the torus, as diagrammed in figure 11. As in the previous cases, the different diagonal O-planes are related to each other by the Gepner symmetry ($\mathbb{Z}_4$). Another peculiarity of this model is that the other involution class, $\alpha = 1 \sim -1$, has species $s = 2$. This is manifest in the O-plane diagram, figure 12, where we can see that this involution results in two disconnected homologous loci. As before there are several different O-planes which fill a Gepner $\mathbb{Z}_4$ multiplet. When examining the formal sublattice

[10] We thank C. Bachas for pointing this out.

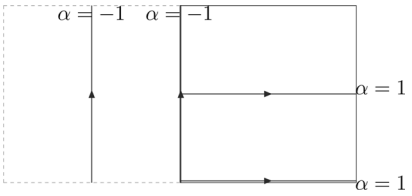

Figure 12: Gepner $(2,2)$ O-planes seen as straight lines. There are two homologous cycles in the $\alpha = 1 \sim -1$ involution class. The fundamental torus is outlined by solid red lines, while the rotated automorphic ones are outlined by hashed orange lines.

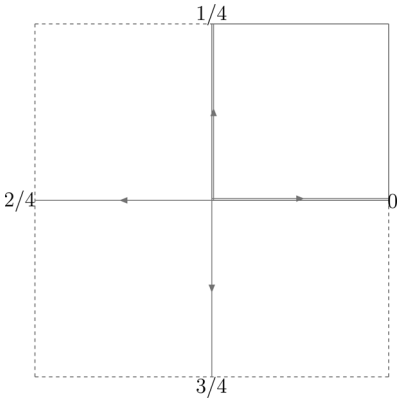

Figure 13: Gepner $(2,2)$ model D-branes seen as straight lines in the torus covering space. The fundamental torus is outlined in solid red lines.

generated by O-plane charge vectors we come upon a surprise. The lattice is now generated by $\{2, 2\tau\}$ (which is a proper sublattic of $\{1+\tau, \tau-1\}$):

- $\alpha = \mathrm{i} \sim -\mathrm{i}$ generated by $\{1+\tau, 1-\tau\}$,
- $\alpha = 1 \sim -1$ generated by $\{2, 2\tau\}$, (actually a proper sublattice of the $\alpha = \mathrm{i}$ case).

For comparison the D-brane results are listed in the same table, table 5. The D-brane charge lattice is generated by $\{1, \tau\}$. The D-branes are diagrammed in figure 13.

One can generate the geometric mirror theory by a simple current extension with $J = p_1 p_2^3 \bmod S$, which is order 2 [35]. As this mirror symmetry extension is even the signs cannot be determined completely resulting in an

Table 6: Gepner (2, 2) Model charges and tensions for B-type O-planes and D-branes labeled by K. The entries are normalized by the brane mass which is independent of K.

K	$M^{B,\text{brane}}$	$Q_z^{B,\text{brane}}$	$\sigma_0 M^{B,\text{crosscap}}$	$\sigma_1 Q_z^{B,\text{crosscap}}$
$(-2,-2)_\pm$	1	-1	1	τ
$(-2,2)_\pm$	1	1	1	1
$(-2,4)_+$	1	τ	$\sqrt{2}$	$1+\tau$
$(-2,4)_-$	1	τ	0	0
$(2,4)_+$	1	$-\tau$	$\sqrt{2}$	$1-\tau$
$(2,4)_-$	1	$-\tau$	0	0

extra sign degree of freedom, η, in the mirror charge description:

$$Q_z^{[K]B,\text{crosscap}} = \frac{1}{\sqrt{2}}(Q_z^{[K]} + \eta Q_z^{[JK]}), \tag{4.20}$$

$$Q_z^{B,\text{brane}}(K) = \sqrt{2} Q_z(K). \tag{4.21}$$

The results for the B-side are presented in table 6, where a + or − subscript to the K label distinguish the sign choice for η. Note that the results in the table are normalized by the mass of the D-brane — which is constant for all K. There are two possible charge lattices for the mirror side:

- the lattice generated by $\{1+\tau, 1-\tau\}$,
- and the lattice generated by $\{1, \tau\}$.

The mirror D-brane lattice is generated, as usual, by $\{1, \tau\}$.

4.5 Summary

From studying these examples, we can see that there is a difference in presentation of the charge lattices of the orientifolds for the different models. We expect that this will impose restrictions on the moduli space of the orientifolds. This is clearly different from the D-brane case where the charge lattice has the same generators throughout. What is particularly interesting is how the $\tau = \mathrm{i}$ torus (the (2,2) Gepner model) has a O-plane charge vectors form a basis of a sublattice of index 2. This is related to this torus having species $s = 2$ which is topologically disconnected from other species of orientifolds. Particularly, this lattice disparity between the $\tau = \mathrm{i}$ and the $\tau = \mathrm{e}^{(\mathrm{i}\pi/3)}$ demonstrates that the orientifold theories with Kalb–Ramond anti-symmetric fields valued at $B = 1/2$ and $B = 0$ exist in separate branches in moduli space. In Section 6, we will explore constructions

of toroidal families where these discontinuities in species will require the degeneration of the cycles where the O-planes lie.

5 Free-field formulation

The torus, the simplest Calabi–Yau manifold, is special in that it has a constant flat metric. This fact allows us to explicitly describe the physics at all points in moduli space using the worldsheet sigma model. We will use the NSR free-field formulation to obtain the charges and tensions of the O-planes and D-branes and compare these results with the data garnered from the CFT perspective. Much of what follows is based on the work of Di Vecchia *et al.*, (eg see [65, 66] and references therein) and Walcher [35]. We could also have used the GLSM description of the torus. However, the general connection between this description, and orientifolds at large volume is already addressed in [29]. As far as CY-spaces are concerned, T^2s are special in that we can also use the free-field formulation.

The worldsheet action of a string compactification on a two-dimensional torus is

$$\begin{aligned} S = -\frac{1}{4\pi\alpha'}\int_\Sigma \Big(& (G_{\alpha\beta}\eta^{ab} + B_{\alpha\beta}\epsilon^{ab})\partial_a X^\alpha \partial_b X^\beta \\ & -\mathrm{i}G_{\alpha\beta}\bar\psi^\alpha \rho^c \partial_c \psi^\beta - \mathrm{i}B_{\alpha\beta}\bar\psi^\alpha \rho^3 \rho^c \partial_c \psi^\beta \Big)\, d^2\sigma. \end{aligned} \tag{5.1}$$

We are using the notational conventions of GSW for the fermions, with ρ being the two-dimensional Dirac matrices with $\{\rho^a, \rho^b\} = 2\eta^{ab}$. The worldsheet metric is Minkowski with a negative time component and $\epsilon^{01} = 1$. The spacetime variables, X^α, are real valued and periodically identified with period 1. The T^2 target space metric is [35]

$$G_{\alpha\beta} = \begin{pmatrix} R_1^2 & R_1 R_2 \cos\,\alpha \\ R_1 R_2 \cos\,\alpha & R_2^2 \end{pmatrix}. \tag{5.2}$$

This corresponds to a torus with periods of length R_1 and R_2 meeting at an angle α, with complex structure $\tau = R_2 \mathrm{e}^{\mathrm{i}\alpha}/R_1$. Additionally there is a constant anti-symmetric background field, $B_{12} = -B_{21} = B$. The presence of the B field can be absorbed as a total derivative in the action. This does not affect the Lagrangian locally, so the equations of motion remain the same. However, it does have global or topological effects. From the point of view of the open string, this modifies the boundary conditions, while the closed string sees this as modification of the zero modes.

The variation of this action results in the open string boundary conditions

$$\delta X^J(G_{IJ}\partial_\sigma X^I + \mathcal{B}_{IJ}\partial_\tau X^I)|_{\sigma=0,\pi} = 0, \quad \mathcal{B} = B + 2\pi\alpha' F, \tag{5.3}$$

for the compact directions, $I = 1, 2$ (and similarly for the fermionic variables). Setting $\delta X^I = 0$ corresponds to Dirichlet boundary conditions. A non-zero $\mathcal{B}_{12} \neq 0$ only has consequences when both $\delta X^1 \neq 0$ *and* $\delta X^2 \neq 0$, i.e., for D2 branes or O2 planes, as the anti-symmetry of $\mathcal{B}$ otherwise ensures that the term in parenthesis reduces to the standard Neumann term. This directly implies that the $\mathcal{B}$ field has no effect for D1, O1, D0 or O0 branes and planes.

Using worldsheet duality, these open string boundary conditions define a state in the Hilbert space of the closed string. On the boundary state, $|B\rangle$, the boundary conditions become constraints. Expressed in terms of the standard oscillator expansions, they are

$$\begin{array}{c}(\alpha^\mu_n + R^\mu{}_\nu \tilde{\alpha}^\mu_{-n})|B\rangle = 0, \\ (\psi^\mu_r - \mathrm{i}\eta R^\mu{}_\nu \tilde{\psi}^\nu_{-r})|B,\eta\rangle = 0,\end{array} \quad \begin{cases}\text{NS}: & r \in \mathbb{Z} + (1/2) \\ \text{R}: & r \in \mathbb{Z}\end{cases} \tag{5.4}$$

with

$$R = \begin{pmatrix} R_{(N)} & 0 \\ 0 & R_{(D)} \end{pmatrix}, \quad \begin{cases} R_{(N)} = (G - \mathcal{B})^{-1}(G + \mathcal{B}), & \text{Neumann directions} \\ R_{(D)} = -\mathbb{1}\ , & \text{Dirichlet directions} \end{cases}. \tag{5.5}$$

Here α^μ_n is the nth mode in the μ direction of the bosonic coordinate X^μ. The ψ^μ_r's are the oscillator modes of the fermionic coordinates, whose boundary conditions can be obtained by supersymmetry from the bosonic ones. The GSO projection will sum over the two spin structures $\eta = \pm 1$. All the boundary information is thus really encoded in the matrix R which is derived from the choice of boundary conditions imposed on (5.3).

We can define the crosscap by an equation analogous to (5.4),

$$(\alpha^\mu_n + (-1)^n R^\mu{}_\nu \tilde{\alpha}^\nu_{-n})|C\rangle = 0 \tag{5.6}$$

$$(\psi^\mu_n - \mathrm{i}\eta(-1)^n R^\mu{}_\nu \tilde{\psi}^\nu_{-n})|C,\eta\rangle = 0. \tag{5.7}$$

In this case the additional $(-1)^n$ factor accounts for the parity action on the crosscap, $\sigma \to \pi - \sigma$. The boundary and crosscap state constraints, (5.4), (5.6) and (5.7) are very similar. For the purposes of our study we are interested in the charges of these states with respect to the Ramond–Ramond ground states. As a result we really only need the solutions to these constraint equations for the zero modes ($n = 0$) of the RR sector. Now, note that the zero modes of both the crosscap and the boundary state satisfy identical defining equations. This implies that the crosscap charges should be a subset of the possible D-brane charges. We will use this to think of the

crosscap charges as generated by a set of D-branes (with the correct charges) placed at the point of involution of the spacetime theory. Consequently this short study applies equally well to O-planes and D-branes, which we will occasionally denote collectively as defect states, $|D\rangle$.

For the torus these boundary and crosscap expressions, (5.4), (5.6) and (5.7) can be explicitly solved yielding these states as coherent sums of oscillators. In the Ramond–Ramond sector the fermion crosscap equation (5.7) is solved by

$$|C\rangle' = -\exp\left[\mathrm{i}\eta\sum_{n=1}^{\infty}(-1)^n\psi_n^\mu R_{\mu\nu}\tilde{\psi}_{-n}^\nu\right]|C,\eta\rangle_0, \tag{5.8}$$

where the zero mode factor $|C,\eta\rangle_0$ must obey

$$(\psi_0^\mu - \mathrm{i}\eta R^\mu{}_\nu\tilde{\psi}_0^\nu)|C,\eta\rangle_0 = 0. \tag{5.9}$$

Following Di Vecchia *et al.* [67] (particularly Appendix A), we can reformulate this requirement in terms of a matrix

$$|C,\eta\rangle_0 = M_{A\tilde{B}}|A\rangle|\tilde{B}\rangle, \tag{5.10}$$

where the $|A\rangle$, and $|\tilde{B}\rangle$ are basis ground state kets transforming under two copies the 32-dimensional SO(1,9) spinor representation of the Ramond oscillator zero modes. Then equation (5.7) applied to the zero modes, reduces to

$$(\Gamma^\mu)^T M - \mathrm{i}\eta(\Gamma_{11})^T M R^\mu{}_\nu\Gamma^\nu = 0, \tag{5.11}$$

where the fermion zero mode action on the RR ground states is represented by two copies of the 32×32 Γ-matrices of SO(1,9): $\psi_0^\mu = \Gamma^\mu\otimes\mathbb{1}$, $\tilde{\psi}_0^\mu = \Gamma_{11}\otimes\Gamma^\mu$ [67]. One finds that the solution to M depends on the number of positive and negative eigenvalues of R, corresponding to the number of Neumann and Dirichlet directions, respectively. For $D-p$ Dirichlet directions in $\mathcal{B}=0$ Minkowski space, M equals

$$M = C\Gamma^0\Gamma^1\ldots\Gamma^p\frac{1-\mathrm{i}\eta\Gamma_{11}}{1-\mathrm{i}\eta} \tag{5.12}$$

with C the charge conjugation matrix.

Finally, the GSO projection in the Ramond sector amounts to averaging over the two $\eta = \pm$ spin structures resulting in,

$$|C\rangle_R = \frac{1}{2}(|C,+\rangle_R + |C,-\rangle_R). \tag{5.13}$$

The full fermionic Linear Sigma-Model Crosscap is thus

$$\begin{aligned} |C\rangle_R = \cos\left[\sum_{r=1}^{\infty}(-1)^r \psi_{-r}\cdot R\cdot \tilde{\psi}_{-r}\right]|a\rangle M_{a\tilde{b}}|\tilde{b}\rangle \\ + \sin\left[\sum_{r=1}^{\infty}(-1)^r \psi_{-r}\cdot R\cdot \tilde{\psi}_{-r}\right]|a'\rangle M_{a'\tilde{b}'}|\tilde{b}'\rangle. \end{aligned} \tag{5.14}$$

where the spin basis $A, \tilde{B}$ has been broken into chiral blocks $a, \tilde{b}, a', \tilde{b}'$ after the GSO projection. Of course, since we are interested in measuring the overlap with the RR ground state zero modes, only the zero mode part encoded in the matrix $M_{a\tilde{b}}$ will be relevant for our study.

Similar to the RR-charges of the O-plane, one can ask about their tensions. We will use the shortcut that the tension can be directly found from the Born–Infeld action, rather than using the NS–NS-sector defect state. It is of course factually the same computation [19].

5.1 A-planes: O1

As mentioned earlier under equation (5.3) the $\mathcal{B}$-field only affects the boundary conditions when none of the directions are Dirichlet. In this section, we will examine the behavior when one of the directions satisfies Dirichlet and the other Neumann boundary conditions. From the point of view of the two torus such a brane wraps a middle-dimensional cycle. Such cycles must corresponds to a special Lagrangian submanifold. As they are one-dimensional they appear as lines in the torus covering space. The special Lagrangian property means that they have minimal volume — so that they are straight lines. Different submanifolds can thus be parametrized by the angle, θ, that they make with the R_1 axis. Generally one can also shift the position of the cycle, but since we want to apply the results to O-planes we will assume that the cycle starts at the origin of the lattice. Using the argument that in the Linear Sigma Model the O-plane charges can be thought of as a stack of D-branes, we can start our O1-plane study by examining D1-branes at different angles θ. O-planes are thus also expected to "wrap" a special Lagrangian submanifold. Indeed the most well known way to construct SLAGs is as the fixed point of an anti-holomorphic involution. However, the O-planes only exist for those SLAGs which truly are the fixed points of involutions.

As discussed by Walcher [35] the angle θ with which D-branes wrap is not arbitrary, but has to be compatible with the description of the torus in the $\mathbb{R}^2$ covering plane. In other words, the cycle, $\hat{\gamma}$, upon which the brane wraps has to close upon itself. This implies that there exist integers n, m such that

$$\tan\,\theta = \frac{nR_2 \sin\,\alpha}{mR_1 + nR_2 \cos\,\alpha}, \tag{5.15}$$

which corresponds to $\hat{\gamma}$ wrapping the R_1 cycle m times and the R_2 cycle n times. This cycle can be described by a displacement vector, $L^I = (m, n)$, of length, $|L|^2 = L \cdot G \cdot L = (mR_1)^2 + (nR_2)^2 + 2mnR_1R_2 \cos\,\alpha$. We will see that these (m, n) are the charges of the D-brane.

The R matrix for these one-dimensional rotated defect states is

$$R_{IJ} = \begin{pmatrix} R_1^2 \cos(2\theta) & R_1R_2 \cos(2\theta - \alpha) \\ R_1R_2 \cos(2\theta - \alpha) & R_2^2 \cos(2\theta - 2\alpha) \end{pmatrix}. \tag{5.16}$$

The easiest way to obtain this matrix is by starting in an orthogonal frame x^i. A suitable change of basis is given by, $e_I{}^i = \begin{pmatrix} R_1 & 0 \\ R_2 \cos\,\alpha & R_2 \sin\,\alpha \end{pmatrix}$, where the orthogonal coordinates are lowercase and the indices likewise lowercase roman letters. One can then start out in an orthogonal frame where x^1, x^2 are chosen to satisfy Neumann and Dirichlet boundary conditions, i.e., $R_{11} = -R_{22} = 1, R_{12} = 0$, rotate to obtain a generic inclined defect state, and then finally change basis to the natural torus coordinates. The choice of boundary conditions encoded in the R matrix identifies the defect state as being A-type. The (left-moving) $U(1)$ charge is measured by the operator $J = \mathrm{i}\epsilon_{\alpha\beta}\psi^\alpha\psi^\beta$ with $\epsilon_{\alpha\beta}$ the Levi–Civita tensor of the spacetime torus. Its eigenvalue on the defect state returns equals minus the product of R eigenvalues. Hence, one has $J|D\rangle = \bar{J}|D\rangle$, identifying the boundary state as being A-type.

The corresponding RR ground state solution to equation (5.11) is thus given by[11]

$$M_{ab} = C\Gamma^0(\Gamma^1 R_1 \cos\,\theta + R_2 \cos(\alpha - \theta)\Gamma^2). \tag{5.17}$$

Here Γ^1, Γ^2 are in the basis (5.2); the metric is therefore not diagonal with regard to the anti-commutation relations for the Γ matrices. The defect state couples to RR 2-form fields with polarizations in the 01 and the 02 directions. Overlap computations with the Ramond vertex break operators[12]

[11] We are implicitly choosing the remaining seven spatial directions to be Dirichlet.

$$\langle C_n| = \frac{1}{n!4\sqrt{2}}\langle A|\mathcal{A}_{\mu_1\ldots\mu_n}(C\Gamma^{\mu_1\ldots\mu_n})_{A\tilde{B}}\langle\tilde{B}|, \tag{5.18}$$

results in,

$$C_{(1)} = \mu_1\frac{2\sqrt{2}V_{1+1}\sin(\alpha-\theta)}{R_1\sin\,\alpha}\mathcal{A}_{01}\epsilon^{01} + \mu_1\frac{2\sqrt{2}V_{1+1}\sin(\theta)}{R_2\sin\,\alpha}\mathcal{A}_{02}\epsilon^{02}, \tag{5.19}$$

where V_{1+1} is the world volume of the defect and arises from the delta functions in the bosonic sector of the defect state [65]. These boundary state techniques do not yield the overall normalization of the state [66]. Moreover this normalization is different for the Ramond and the NS sectors of the theory. Different techniques can be used to explicitly obtain these normalizations. However, for our purposes it will be sufficient to absorb this ambiguity in the charge density, μ_1. We will absorb the $2\sqrt{2}$ factor as well. Later we will check the consistency of our choice by examining the BPS condition.

We have thus found the O1-plane charges

$$Q^{01} = V_{1+1}\frac{\sin(\alpha-\theta)}{R_1\sin\,\alpha}, \quad Q^{02} = V_{1+1}\frac{\sin(\theta)}{R_2\sin\,\alpha}. \tag{5.20}$$

One can rewrite this in more recognizable form by replacing the world-volume, V_{1+1}, by the cycle length, L. After some simplification using $L = |(m,n)|$, and (5.15), one obtains the charges,

$$Q^{01} = m, \quad Q^{02} = n, \tag{5.21}$$

which precisely corresponds to a decomposition of the plane cycle, $\hat{\gamma} = m\hat{\alpha} + n\hat{\beta}$, in terms of the standard torus homology basis (that is the R_1 and R_2 cycles.) The charges, (m,n), then count the number of cycles in the two different torus homology classes around which the O1-plane/D1-brane wraps. These are the same charges which were obtained in Section 4, whereupon the CFT calculation identified the charges with the cohomology elements dual to these cycles.

It is now a trivial check on our computations to verify that the answer BPS. The absolute value of the charge is proportial to the length of the D-brane

$$Q.G.Q = L^2, \tag{5.22}$$

and the latter is the mass divided by the tension.

[12]Note the normalization,

$$\langle C_n|C_n\rangle = \frac{\mathcal{A}^{\mu_1\cdots\mu_n}\mathcal{A}_{\mu_1\cdots\mu_n}}{n!}.$$

5.2 B-planes: O2/O0

By choosing the modified Neumann boundary conditions in equation (5.3) for both directions one can construct two-dimensional boundary states. By the same reasoning as above, we will assume that the O-plane can be considered a superposition of boundary states at the point of involution. The boundary conditions are now encoded in the matrix,

$$R_{ij} = \frac{1}{1+b^2}\begin{pmatrix} 1-b^2 & 2b \\ 2b & 1-b^2 \end{pmatrix}, \tag{5.23}$$

where orthogonal coordinates have been used to produce a simpler expression. In this basis, $\mathcal{B} = \mathcal{B}_{12} = bR_1R_2 \sin\,\alpha$. The R matrix now has two positive eigenvalues, so the defect state is of B-type.

The corresponding Ramond ground state information is then contained in the matrix [66]

$$M_{ab} = C\Gamma^0(\Gamma^1\Gamma^2 R_1R_2 \sin\,\alpha + \cot\,\alpha + \frac{\mathcal{B}}{R_1R_2 \sin\,\alpha}), \tag{5.24}$$

where we have switched to natural torus coordinates (5.2). From this expression, it is evident that the O2-plane/D2-brane can couple to a Ramond 1 form, $C_{(0)}$ and to a three form, $C_{(2)}$. Computing the overlap with the corresponding vertex operators gives the coupling

$$C_{(2)} = \frac{2\sqrt{2}\mu_2 V_{2+1}}{R_1R_2 \sin\,\alpha}\mathcal{A}_{012}\epsilon^{012}, \tag{5.25}$$

for the three form and

$$C_{(0)} = \frac{2\sqrt{2}\mu_2 V_{2+1}\mathcal{B}}{R_1R_2 \sin\,\alpha}\mathcal{A}_0 \tag{5.26}$$

$$= \frac{\mu_2 V_{2+1}}{R_1R_2 \sin\,\alpha}\mathcal{A}_0\frac{\mathcal{B}_{ij}\epsilon^{ij}}{2!}, \tag{5.27}$$

for the 1-form. Note that μ_2 will be used to absorb the $2\sqrt{2}$ factor as before. If we replace the world volume term, V_{2+1} by the size of the D2-plane/O2-plane, $NR_1R_2 \sin\,\alpha$, where N counts the number of wrappings around the torus, we can extract the charges

$$q_2 = N, \tag{5.28}$$

$$q_0 = N\mathcal{B}. \tag{5.29}$$

Intuitively, we can relate q_2 to the number of 2-cycles of the torus, which by Poincare duality, counts the charge in the dual cohomology class of $dZ \wedge d\bar{Z}$.

The q_0 number counts the amount of magnetic flux. This can be attributed to the Wess–Zumino term [66, 68]

$$\mu_p \int_{\mathcal{M}_{p+1}} \left(\sum_p C_{p+1} \right) \wedge \mathrm{e}^{2\pi\alpha' F + B} \tag{5.30}$$

in the generalized defect action which shows how the magnetic flux can manifest itself as dissolved D0-branes/O0-planes.

The role of the induced D0/O0 charge can be understood by T-dualizing the theory along an axis orthogonal to X^1. If we then make the identification $\mathcal{B} \to -R_1 R_2 \sin\alpha \tan\theta$, or equivalently $q_0/(R_1 R_2 \sin\alpha) \to -\tan\theta$, we obtain the R and M matrices corresponding to an O1-plane/D1-brane inclined at angle θ, quantized as described in the previous section. In other words, for a given inclination of the D1-brane/O1-plane, the relative number of $\hat{\beta}$ to $\hat{\alpha}$ cycles manifests itself as magnetic flux or D0/O0-plane charge in the T-dual picture. We have thus implicitly captured the pure D0-brane description as well. Recalling also that T-duality on a torus is mirror symmetry, the above has simultaneously verified the connection with the CFT results in the previous section.

As a quick check we can compute the BPS condition. Using the natural inner product on vertical cohomology charge vectors,

$$q_0^2 + q_2^2 \det G = M^2, \tag{5.31}$$

we find agreement with the Born–Infeld factor for N D-branes or O-planes

$$N\sqrt{\det(G + B + 2\pi\alpha' F)} = N\sqrt{(R_1 R_2 \sin\alpha)^2 + \mathcal{B}^2}. \tag{5.32}$$

6 Discussion and outlook: towards elliptic fibrations

The tori we studied in Section 4 are naturally described as elements of different algebraic families. In this section, we wish to examine how the involutive maps which give rise to the T^2 orientifolds can be compatibly extended to such families. In particular, this demands some action on the base which we will discuss later. We will restrict our study to anti-holomorphic maps so as to take advantage of existing mathematical results on anti-analytic maps on Riemann surfaces. Since we are ultimately interested in applications to string compactifications, we will require that the total space of the algebraic family be an elliptically fibered $K3$ surface.

Geometrically we expect that the $K3$ O-planes associated with each orientifold can be characterized, to some degree, in terms of their RR charges

by D-branes which wrap the fixed point locus. We will use known mathematical results on real submanifolds of $K3$'s to validate our results [69–71]. The analysis is by no means exhaustive: our goal is only to illustrate how the simple results of tori O-planes may be generalized to richer geometric constructions in higher dimensions.

In this paper, we deal with two elliptically fibered $K3$'s in detail:

- a simple example — the "linear model",
- the sextic.

The first item is a simple model which exemplifies the techniques and ideas used. The next one is a pencil family containing the (1,4) Gepner model which extends the analysis of the linear toy example to a more realistic one and introduces some interesting points in the construction of $K3$ involutions. Two families, the quartic and the cubic, which contain the other two Gepner model are technically more complex and will be briefly discussed in the appendices.

Each torus of the family is characterized by its J-invariant. The J-invariant may take an infinite value in the limit that the elliptic curves become singular. Singular fibers in elliptic fibrations have been classified by Kodaira, and correspond in a natural way to the ADE classification of extended Dynkin diagrams. In his notation a smooth elliptic curve is of type I_0, a nodal rational curve is of type I_1, a cycle of N smooth rational curves is of type I_N (Dynkin type A_{N-1}), a cuspidal rational curve is of type II, a configuration of two tangent rational curves are of type III (type A_1), and three concurrent rational curves are of type IV (type A_2). There are also "quadratic twisted" versions of all of these: I_0^* (Dynkin type D_4), I_N^* (type $D_{N>4}$), IV^* (type E_6), III^* (type E_7), and II^* (type E_8). The J-invariant takes infinite values at fibers of types I_N and I_N^* with $N \geq 1$, and finite values at all other singular fibers. The J-invariant vanishes at singular fibers of types II, IV, IV^* and II^*. It takes value 1 at fibers of types III and III^*. The J-invariant of a singular fiber of type I_0^* can take any finite value whatsoever.

In particular, this means that one can determine the singularity type, if any, of an elliptic curve occurring in a family parametrized by a complex variable w by the ramification behavior of Kodaira's functional invariant $\mathcal{J}(w)$. The function $\mathcal{J}(w)$ maps from base-coordinate w to the J-line, and for an elliptic curve over w_0 to be singular it is necessary that $\mathcal{J}(w_0) \in \{0, 1, \infty\}$. If $\mathcal{J}(w_0) = \infty$ then this is also sufficient. More generally, however this is not the case (see, for example, Lemma 4.5 in [72]). The full story is given in table 7 which correlates the multiplicity $\mu(\mathcal{J})$ of $\mathcal{J}(w)$ at w_0 with

Table 7: Table of Kodaira types.

$\mathcal{J}(w_0)$	$\mu(\mathcal{J})$	Kodaira types	Contribution to Euler Number
0	0(mod3)	I_0 or I_0^*	0 or 6
	1(mod3)	II or IV^*	2 or 8
	2(mod3)	IV or II^*	4 or 10
1	0(mod2)	I_0 or I_0^*	0 or 6
	1(mod2)	III or III^*	3 or 9
∞	pole of order N	I_N or I_N^*	N or $N+6$

the Kodaira singularity types. Thus given the functional $\mathcal{J}$-invariant of a family of elliptic curves, we can determine which members are singular and have multiple representatives for the same value of J. The last column in table 7 lists the contribution of each singularity to the Euler number of the total space formed by the family of elliptic curves. For $K3$ surfaces this must be equal to $\chi = 24$.

To construct a type A $K3$-orientifold from an elliptically fibered $K3$ surface through an anti-holomorphic involution (both on the base and the fiber), recall from Section 2 that the requirement for the existence of a torus with anti-holomorphic map is that the J-invariant be real. The orientifold family associated to the torus family is then the pullback of the $\mathcal{J}$-section to the real numbers combined with the datum on the choice of involution (the choice of involution type within each species branch). This choice may be constrained by compatibility requirements over the family. In the case of the standard $w \to \bar{w}$ action on the base, the discriminant, given by equation (2.13), identifies the choice on each branch. Regardless, it is then noteworthy that there is a global disconnect in the choice of species of involution at $\mathcal{J} = 1$. The species number is a topological property of the fixed point locus corresponding to the O-plane. Within a family the species could therefore be affected by the singular fiber structure of the family, which is reflected in the $\mathcal{J}$-invariant global choice that the overall space is a $K3$ and the choice of involution on the base. As we will show now, in an illustration of the power of geometrical insight, this is generally the case.

6.1 The linear model

Consider the elliptic family whose J-invariant simply given by

$$\mathcal{J}(t) = t. \tag{6.1}$$

This family has singular fibers IV^*, III^* and I_1^* located at $t = 0$, 1 and ∞, respectively, with Weierstrass form parametrized by

$$g_2 = 3t^3(t-1)^3, \tag{6.2}$$

$$g_3 = t^4(t-1)^5. \tag{6.3}$$

These and the other families were constructed using the methods described in [73]. As mentioned earlier a torus admits anti-holomorphic maps whenever its J-invariant is real. In this simple case, the pullback of the J-invariant is just the restriction that Im $t = 0$. This follows from the restriction of the standard anti-holomorphic involution on the ambient $\mathbb{P}^2$ bundle over $\mathbb{P}^1$ to the subspace described by Weierstrass equation. The restriction to the base is then the standard anti-holomorphic map $t \to \bar{t}$, with fixed point set given by t real. Since the pullback of the $\mathcal{J}$-invariant is a single cover of $\mathbb{P}^1$ we call this model the "linear" one. Given that the $\mathcal{J}$-invariant pullback is simply connected it would seem naively that the orientifold moduli space would also be connected. However, in order to describe the orientifold, in addition to the J-invariant, we need to specify the type of involution. The space of involutions has a topological disconnect at $\mathcal{J} = 1$ (see figure 3): for $\mathcal{J} < 0$ there only exists species $s = 1$ involutions while for $\mathcal{J} > 0$ one has either $s = 2$ or fixed point free $s = 0$ involutions. This seems to indicate that there must be some sort of degeneration of cycles along the path Im $t = 0$ as this otherwise smooth path traverses the topological discontinuity at $\mathcal{J} = 0$. This degeneration of fixed point cycles is seen to occur at some of the Kodaira singular fibers as described by Silhol [70] and appears to be a generic phenomenon in these toroidal families.

Silhol [70] analyzed the possible transitions of cycles along paths given by real parameters for real elliptic curves. His conclusions were that the species number could jump only over singularities of type I_n^*, for n odd, or over those of type III^*. By plotting the real loci of the Weierstrass equation, $Y^2 = 4X^3 - g_2(t)X - g_3(t)$ it is apparent that there is a single fixed point locus for $\mathcal{J} < 0$ which splits into two branches at the I_1^* fiber located at minus infinity. Wrapping around and progressing from positive infinity towards $\mathcal{J} = 1$ we see that one of the cycles begins to shrink until it finally "caps off" at $\mathcal{J} = 1$. We can continue uninterrupted from $\mathcal{J} = 1$ until $\mathcal{J} < 0$ with no further exceptional behavior. There is no degeneration of the real locus over the IV^* fiber located at $\mathcal{J} = 0$. This behavior is shown schematically in figure 14.

We can connect these results with the known properties of anti-holomorphic involutions on the full $K3$. In particular, the anti-analytic fixed point loci of $K3$ surfaces have been studied [69, 71]. These loci can be classified according to some topological characteristics relating to the action

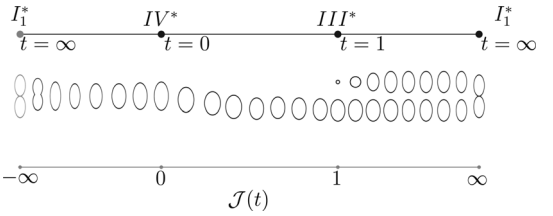

Figure 14: The linear model J-line pullback with a cartoon depicting the degeneration of the real loci.

of the involution on the $K3$ lattice. It was found that (with two exceptions) they correspond to the union of a genus g surface with k copies of S^2 (the two sphere). Figure 15 of the fixed point locus on the $K3$ shows how the base fixed point locus supports a genus 1 curve, so $g = 1$. The 2-cycles represented by copies of S^2 are not necessarily purely transcendental or algebraic in nature and we should not expect to see these additional fixed point locus components in the Weierstrass presentation. The precise relationship between the lattice-theoretic description of anti-holomorphic involutions on $K3$ surfaces and elliptic fibrations with section on $K3$ surfaces will be studied carefully in future work.

Generically, we have found that as the standard involution on the base results in a base fixed point locus which is topologically a circle, the fixed point locus in the fiber sweeps out a curve which is at least of genus 1. This is compatible with the Nikulin classification [69]. The trivial base involution arises from restriction of the standard anti-holomorphic map on the ambient space. However, it may be possible to find other anti-holomorphic maps and the corresponding orientifolds. This is exemplified by the Sextic model considered below.

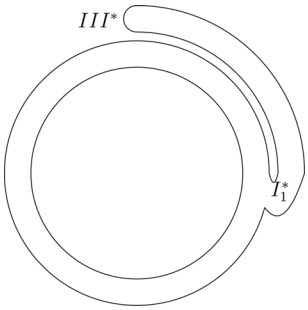

Figure 15: Schematic diagram of the topological structure of the involution fixed point locus for the $\mathcal{J} = t$ model.

6.2 The sextic pencil

The next example is the family corresponding to the pencil containing the sextic hypersurface

$$x_1^6 + x_2^3 + x_3^2 - z^{-1/6} x_1 x_2 x_3 = 0 \text{ in } \mathbb{WP}^2_{1,2,3}. \tag{6.4}$$

This family contains the Gepner model (1,4) at $z = \infty$ [74].[13] Although the natural parameter describing this family is $w = -2^4 3^3 z$, it is advantageous to make the $\mathrm{PSL}(2,\mathbb{Z})$ transformation $t = (w - 1/w)$ to obtain the Weierstrass parameters in polynomial form,

$$g_2(t) = 3(t-1)^4 t^2, \tag{6.5}$$

$$g_3(t) = (t-1)^5 t^3 (t+1). \tag{6.6}$$

The $\mathcal{J}$-invariant is given by

$$\mathcal{J}(t) = -\frac{1}{4}\frac{(t-1)^2}{t}, \tag{6.7}$$

or as

$$\mathcal{J}(t) = -\frac{1}{4w(w-1)}, \tag{6.8}$$

in terms of the natural pencil parameter. This family has two I_1^* singularities at $w = 0$ and $w = 1$ and a type II^* fiber at $w = \infty$. The $\mathcal{J}$-invariant is a little more complicated than the previous case. The pullback in this case is double cover of $\mathbb{P}^1$ with ramification points at $w = 0$ and at $w = \infty$. The pullback is illustrated in figure 16 and a summary of the behavior of the w parameter on each path is given in the accompanying table.

An analysis similar to that of the linear model can be made for the regions where the pencil parameter, w (or equivalently t), is real. As explained earlier, this base locus arises by simply considering the restriction of standard anti-holomorphic map on the ambient space ($x_i \to \bar{x}_i$) to the $K3$. This real w-locus corresponds to the region where $\mathcal{J} < 0$ and $\mathcal{J} > 1$. In figure 16, this is a loop delimited by the legs labeled A, E, F and B. Along the leg A one has a single cycle that splits at the I_1^* fiber as $\mathcal{J} \to -\infty$ ($w \to 0$). The two resulting cycles then travel along the legs E and F to recombine at the other I_1^* fiber as $\mathcal{J} \to \infty$ ($w = 1$). These cycles do not transition to the $\mathcal{J} < 1$ region at the ramification point $w = \frac{1}{2}$ as there is the aforementioned topological discontinuity dividing the J-line into regions solely admitting $s = 1$ involutions (for $\mathcal{J} < 1$) and those allowing $s = 0, 2$ loci for $\mathcal{J} > 1$. Back along the leg B the single cycle rejoins that of path A at the ramification point $w = \infty$. This ramification point does contain a singular

[13] This paper lists the families containing the Gepner models we studied, however, they seem to have a sign difference in the z term.

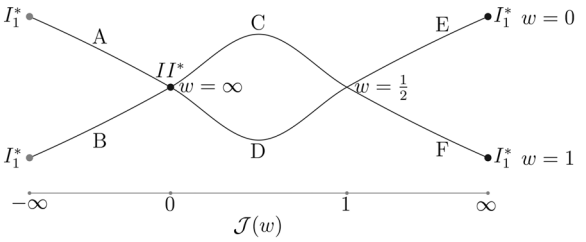

Segment	$-\infty$		0		1		∞
A		real 0 to $-\infty$					
B		real 1 to ∞					
C				complex ∞ to $\frac{1}{2}$ constant real part			
D				conjugate ∞ to $\frac{1}{2}$			
E						real $\frac{1}{2}$ to 0	
F						real $\frac{1}{2}$ to 1	

Figure 16: The pullback of the real $\mathcal{J}$-invariant for the sextic family.

fiber of type II^*, though as shown by Silhol [70] this does not result in a degeneration of the real locus, or change of species. This can be verified by simply plotting the Weierstrass equation along the path. The path ABEF where the pencil parameter is real hence contributes a genus $g = 2$ to the fixed point locus of the $K3$. The resulting fixed point curve is shown schematically in figure 17.

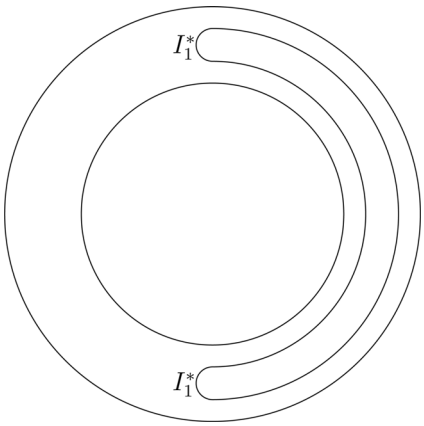

Figure 17: Schematic diagram of the topological structure of the involution fixed point locus for the Sextic. The handle on the left hand side corresponds to the AB branch on the base parameter locus, while the double handle on the right is the EF fixed point locus (of species type 2). The fixed point curve is of type $g = 2$.

One major difference with the simple model studied earlier is the existence of a central loop CD (i.e., for $0 < \mathcal{J} < 1$) where w is complex valued. The values of w along one branch are conjugate to the those of the other branch. Since w is complex the Weierstrass equation has complex coefficients and one cannot directly plot it in $\mathbb{R}^2$ to investigate the fixed point loci (as in the linear case). However, we can directly analyze the Weierstrass $X = \wp(u; g_2, g_3)$ and $Y = \wp'(u; g_2, g_3)$ functions. If we let the auxiliary variable u, valued in the torus covering space, lie along the fixed point locus, we find that $\wp$ and $\wp'$ can be independently rotated by an w dependent phase to a real plane. Plotting the rotated variables, we see that the fixed point locus is an $s = 1$ curve. Given a choice of involution on one branch, we need to select the other type involution for the complex branch in order to have matching curves at the ramification points. As this w-locus is complex it is clearly not fixed by the standard anti-holomorphic map inherited from the ambient space. The standard involution instead maps one complex branch to its conjugate. In terms of the w parameter the complex branches are described by $w = (1/2) \pm \mathrm{i}v$ with $v \in (0, \infty)$. We can make a general linear transformation to reparametrize the C and D branches so that they are described by the real parameter $v = \pm\mathrm{i}(w - 1/2)$. As this new parameter is real, it is fixed by some canonical extended anti-holomorphic map. The linear transform also results in the legs A, B, E and F being now described by complex parameters which consequentially are not fixed under the new involution. Since the base is $\mathbb{P}^1$, the restriction of the anti-holomorphic involution on the ambient space should restrict to an involution on the base, which is $w \to \pm\bar{w}$ modulo $\mathrm{PGL}(2, \mathbb{C})$. The more suitable question is whether one can find the $K3$ involution from which this base involution emerges. Regardless of the specific details of the involutive map, we can determine that the complex CD loop supports a genus $g = 1$ curve.

The linear case has exemplified how the real locus on the base supports a genus g curve, consistent with Nikulin's classification of fixed point loci in $K3$ surfaces. The reality of the base parameter can be seen to be the result of restricting the standard ambient anti-holomorphic involution to the base of the $K3$. The sextic, a more realistic and relevant example, demonstrates that the parameter space where the elliptic fibers admit involutions is typically larger than the space where the base parameter is real. Such loci ought to correspond to other anti-holomorphic involutions on the $K3$ with non-trivial action on the base. The question then is to find and classify these other involutions. The other families relevant to our paper, the quartic and cubic, are more complicated in the branching and ramification of the pullback of the real $\mathcal{J}$-line. Like the linear and the sextic model the real locus on the base supports a genus g curve. However, there are more complex and

complex conjugate branches which might be fixed under other non-standard anti-holomorphic involutions. A brief account of the real base parameter locus for these other families is presented in the adjoining appendices. It is our hope to extend this study in a subsequent paper where we may be able to more systematically analyze the possible involutions and orientifolds in $K3$'s.

6.3 Conclusion and outlook

Orientifold compactifications in string theory provide a very rich and promising phenomenological playground. Toroidal compactifications are still the most well understood starting point for orientifold compactifications. The goal is to understand them more generally. One road of approach is to deform away from the toroidal point in moduli space [75]. Another is the worldsheet gauged linear sigma model approach to better understand the quantum geometry [28–30]. The preview towards orientifolds of elliptically fibered compactifications in this section points to a third way. It is one of the main motivations for the study undertaken here. In any of these T^2-compactifications play an essential role, either as building block or example. They stand out due to their simplicity. As we illustrated in this article, this allows a deep connected and complementary understanding of various geometric or worldsheet approaches to T^2-orientifolds, which should aid us in developing a general understanding of these mysterious quantum objects.

Acknowledgments

We are very grateful to the hosts and participants of the Simons Workshop in Mathematical Physics (Stony Brook, 2003). In particular, we wish to thank Christian Römelsberger and Cumrun Vafa. We also thank Jan de Boer, Kentaro Hori and Bert Schellekens for useful comments, and especially Lennaert Huiszoon and Brian Greene who were originally part of this collaboration. A number of calculations were checked with Bert Schellekens' program `kac` (http://www.nikhef.nl/∼t58/kac.html), an indispensable tool. K.S. is grateful for partial support from DOE grant DE-FG-02-92ER40699 and from a VIDI Innovational Research Incentives Award of the Netherlands Organisation for Scientific Research (NWO).

Appendix A

A Families of the (2,2) and (1,1,1) Gepner orientifolds

For completeness we briefly analyze the elliptic $K3$-orientifolds based on families of the (2,2) and the (1,1,1) Gepner orientifolds.

A.1 The quartic pencil

The family containing the quartic hypersurface is described by

$$x_1^4 + x_2^4 + x_3^2 - z^{-1/4} x_1 x_2 x_3 = 0 \text{ in } \mathbb{WP}^2_{1,1,2}. \tag{A.1}$$

The variable $w = 2^6 z$ parametrizes the complex structure moduli of this weighted quartic. In the limit that $w \to \infty$ we get the Gepner model (2,2) studied in Section 4. As before, we can change variables to $t = (w - 1/w)$ to obtain the Weierstrass parameters in polynomial form:

$$g_2(t) = 3t^2(t-1)^3(t-4),$$
$$g_3(t) = t^3(t-1)^5(t+8).$$

In terms of this new parametrization the $\mathcal{J}$-invariant reads

$$\mathcal{J}(t) = -\frac{1}{27}\frac{(t-4)^3}{t^2}, \tag{A.2}$$

or in terms of w we have,

$$\mathcal{J}(w) = \frac{(1+3w)^3}{27w(1-w)^2}. \tag{A.3}$$

This family has singularities of types I_1^*, I_2^* and III^* at $w = 0$, 1 and ∞. The locus with $\mathcal{J}$ real is visibly a triple cover of the real J-line, as indicated in figure A1.

There are two type of paths: paths parametrized by real w which can be directly analyzed as in the linear model, and pairs of paths corresponding to complex w and its conjugate. Focusing on the real path we can start at $w = -\infty$ and follow the progression of increasing w. This is schematically illustrated in figure A2. As described by Silhol [70] along the CD branch the locus varies smoothly until it splits at the I_1^* singularity located at $w = 0$ ($\mathcal{J} \to -\infty$) in agreement with the topological distinction between $s = 1$ involutions for $\mathcal{J} < 1$ and $s = 2, 0$ for $\mathcal{J} > 1$. The cycle pair then vary along legs KHG until one of them is capped off at the III^* fiber located at $w = \infty$. The change in fixed point topology here has been mentioned by Silhol [70] and is the same mechanism that allows us to align the topological

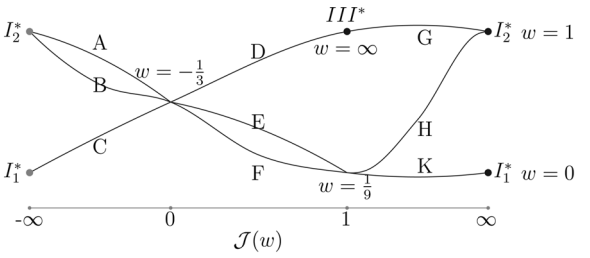

Segment	$-\infty$		0		1		∞
A		complex 1 to $-\frac{1}{3}$					
B		conjugate 1 to $-\frac{1}{3}$					
C		real 0 to $-\frac{1}{3}$					
D				real $-\frac{1}{3}$ to $-\infty$			
E				complex $-\frac{1}{3}$ to $\frac{1}{9}$			
F				conjugate $-\frac{1}{3}$ to $\frac{1}{9}$			
G						real ∞ to 1	
H						real $\frac{1}{9}$ to 1	
K						real $\frac{1}{9}$ to 0	

Figure A1: The quartic.

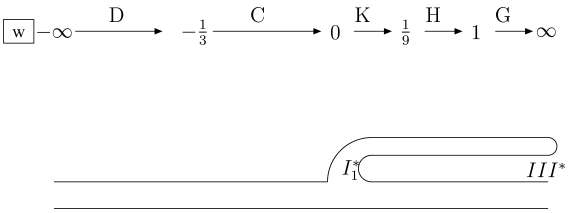

Figure A2: Schematic diagram of the topological structure of the involution fixed point locus of the Quartic for the standard $K3$ involution (i.e., with standard action on base). The ends of the figure are identified. The fixed point curve is of type $g = 1$.

discontinuity of involution over the $\mathcal{J}$-line with the smooth family picture. This real locus is very similar to the linear model case and contributes a handle to the fixed point locus.

Presumably one could find other involutions on the $K3$ which would fix the complex w base branches. It would be interesting to know whether both complex loops, AB and EF, could be fixed simultaneously or not. Since path EF does not cross any intersections and supports $s = 1$ fixed loci on its fibers it clearly yields a contribution of 1 to the $K3$ fixed curve genus. More analysis is required.

A.2 The cubic pencil

The T^2 underlying the $(1,1,1)$ Gepner model, also known as the "cubic", is the hypersurface described by

$$x_1^3 + x_2^3 + x_3^3 - z^{-1/3} x_1 x_2 x_3 = 0 \text{ in } \mathbb{P}^2 \tag{A.4}$$

The variable $w = 3^3 z$ parametrizes the complex structure moduli of the cubic. There are I_1^*, I_3^* and IV^* singular fibers at the points $w = 0$, 1 and ∞. The change of variables $t = ((w-1)/w)$ yields the Weierstrass parameters:

$$g_2(t) = 3t^2(t-1)^3(t-9),$$
$$g_3(t) = t^3(t-1)^4(t^2+18t-27),$$

with $\mathcal{J}$-invariant

$$\mathcal{J}(t) = -\frac{1}{64}\frac{(t-1)(t-9)^3}{t^3}. \tag{A.5}$$

In terms of the pencil parameter the $\mathcal{J}$-invariant is

$$\mathcal{J}(w) = \frac{(1+8w)^3}{64w(1-w)^3}. \tag{A.6}$$

This time the restriction to real J-values yields a triple cover of the J-line. This is shown in figure A3.

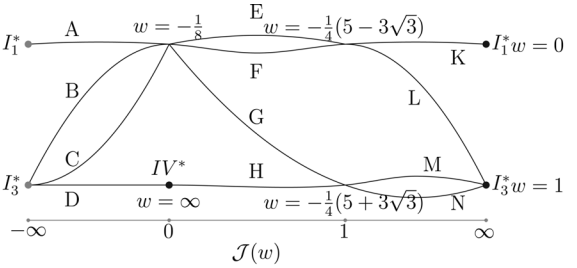

segment	$-\infty$		0		1		∞
A		real 0 to -1/8					
B		complex 1 to -1/8					
C		conjugate 1 to -1/8					
D		real 1 to ∞					
E				complex -1/8 to 0.49			
F				conjugate -1/8 to 0.49			
G				real -1/8 to -2.55			
H				real $-\infty$ to -2.55			
K						real 0.49 to 0	
L						real 0.49 to 1	
M						complex -2.55 to 1	
N						conjugate -2.55 to 1	

Figure A3: The cubic.

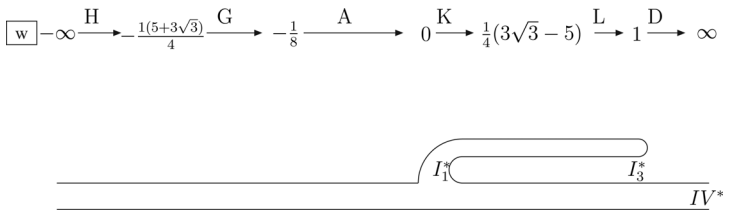

Figure A4: Schematic diagram of the topological structure of the standard (i.e., with standard base action) involution fixed point locus for the Cubic. The ends of the figure are identified. The fixed point curve is of type $g = 1$.

The overall result is similar to the quartic family. As in the sextic case the appearance of complex loops in the base which can support fixed loci on their fibers indicates the possibility of involutions with non-trivial action on the base. For simplicity, we will focus on involutions which restrict to w standard action on the base. Following the real path of the parameter w, starting from $-\infty$ we have a single cycle along the H leg. As Silhol [70] shows, the IV^* fiber does not degenerate the real cycle. At the $w = -(1/8)$ ramification we continue along the real path A reaching a splitting point induced by the fiber I_1^* at $w = 0$. The resulting cycle pairs travel along KL, in accordance with this region having $s = 2$, until one of them caps off a the I_3^* fiber at $w = 1$. The remaining real cycle then continues along D to return to its starting point. The resulting $K3$ fixed locus component has genus $g = 1$. This is schematically shown in figure A4.

B *P*-matrix entries in Gepner models

We seek explicit expressions for Gepner model P-matrix entries with one index corresponding to that of a chiral field and the other to a Klein Bottle current of the $\mathcal{A}^{\text{ws}}$ theory. The $\mathcal{A}^{\text{ws}}$ model is obtained as a simple current extension from the tensor product of r minimal models and a $D_{8-n,1}$ WZW model. This simple current extension, commonly referred to as "fermion alignment", is responsible for ensuring that there is a well-defined worldsheet supersymmetry.

In terms of the constituent P-matrices, the P-matrix of a simple current extension is

$$P_{[a],[b]} = e^{\pi \mathrm{i}(a_{[a]}+a_{[b]})} \sum_{n=1}^{N} \epsilon_{J^n}(b) P_{a,J^n b}. \tag{B.1}$$

The phases $\epsilon_{J^n}(b) \equiv \mathrm{e}^{\pi i(h_b - h_{J^n b})}$ and $a_{[a]} = h_{[a]} - h_a$ (the difference between the true conformal weight $h_{[a]}$ of the orbit $[a]$ and that of the chosen representative element) ensure that expression for the P-matrix is invariant on orbits $[a]$. For convenience the phase factor, $\mathrm{e}^{\pi \mathrm{i}(a_{[a]}+a_{[b]})}$, will be dropped in the intermediate steps to the final answer. With regard to its modular properties, each minimal model, represented as a $\mathrm{SU}(2)_k \times U(1)_4/U(1)_{2\mathfrak{h}}$ coset can be thought of as an $\mathrm{SU}(2) \times U(1)^* \times U(1)$ tensor product extended by an order two simple current, whose orbits impose *field identification* $(l, m, s) \Leftrightarrow (k - l, m + \mathfrak{h}, s + 2)$.

The NS Klein bottle currents of the $\mathcal{A}^{\mathrm{ws}}$ theory are the orbits $[G^{NS}_{8-d,1}[0; \vec{n}; \vec{m}]]$ with both n_i and m_i even. Fermion alignment can be used to reduce all the $m_i = 0$. The (anti)-chiral fields of the minimal model are the fields $(l, l', 0)$ where $l' = \pm l$.

Recall the forms of the $\mathrm{SU}(2)_k$ and $U(1)_{2\mathfrak{h}}$ P-matrices

$$P^{\mathrm{SU}(2)_k}_{l_1,l_2} = \frac{1}{\sqrt{\mathfrak{h}}} \sin\left(\frac{\pi(l_1+1)(l_2+1)}{2\mathfrak{h}}\right) \sum_{u=0}^{1} (-1)^{u(k+l_1+l_2)}, \quad \mathfrak{h} = k+2,$$

$$P^{U(1)_{2\mathfrak{h}}}_{m_1,m_2} = \frac{\mathrm{e}^{-(\pi i m_1 m_2/2\mathfrak{h})}}{2\sqrt{\mathfrak{h}}} \sum_{u=0}^{1} (-1)^{u(\mathfrak{h}+m_1+m_2)}. \tag{B.2}$$

Due to the selection rule $k + l_1 + l_2 \in 2\mathbb{Z}$ for the $\mathrm{SU}(2)$ P-matrix, odd and even k minimal models behave differently. As l_2 vanishes for *all* Klein bottle currents, this selection rule reduces to $k + l_1 \in 2\mathbb{Z}$. For odd k minimal models therefore only *one* of the elements of the identification orbit contributes, which depends on the nature of l_1. For even k minimal models only $l_1 \in 2\mathbb{Z}$ P-matrix entries are non-zero, but for each both elements of the identification orbit contribute. It is straightforward to check that for (anti)chiral fields $(l, \pm l, 0)$ the $U(1)$ selection rules yield the same conditions.

Explicitly we find the following values for the minimal model P-matrix

$$P^{min}_{(l,\pm l,0),(0,n,m)} = \frac{\sqrt{2}}{\mathfrak{h}} \mathrm{e}^{\pm(\pi i l n/2\mathfrak{h})} \left(\mathrm{e}^{\pi \mathrm{i}((n/2)-(m/2))} \sin\left(\frac{\pi(l+1)}{2\mathfrak{h}}\right) \delta^{(2)}_{k+l} \delta^{(2)}_{m} + \cos\left(\frac{\pi(l+1)}{2\mathfrak{h}}\right) \delta^{(2)}_{l} \delta^{(2)}_{m} \right). \tag{B.3}$$

Owing to aforementioned difference in behavior of the P-matrix as a function of whether k is odd or even, we will first study the cases where all the k_i are purely odd or even. The mixed case can then be built by fermion

aligning a purely even and odd tensor block. Finally we will tensor in the spacetime part.

B.1 Models with all k_i odd

Tensoring r odd k_i minimal models and extending by the currents w_i we obtain the following P-matrix entries for the fermion aligned tensor theory, $\mathcal{A}^r$ theory. (Recall that a representative of an orbit under the w_i has all $s_{i\neq 1} = s_1 \mod 2$, $s_1 = -1, 0, 1, 2$.) We use below that $\epsilon_{v_i}(0, n_i, 0) = \mathrm{i}$ and the following useful relation

$$P^{\text{min, } k \text{ odd}}_{(l,\pm l,0),(0,n,m)} = \mathrm{e}^{-(\pi \mathrm{i} l m/2)} P^{\text{min, } k \text{ odd}}_{(l,\pm l,0),(0,n,0)}. \tag{B.4}$$

$$\begin{aligned}
P^{r}_{[\vec{l};\vec{l}';0],[0;\vec{n};0]} &= \prod_{i=1}^{r} \left(P^{\min,k_i}_{(l_i,\pm l_i,0),(0,n_i,0)} \right) \\
&\quad + \sum_{i<j} \epsilon_{v_i}(0,n_i,0) P^{\min,k_i}_{(l_i,\pm l_i,0),(0,n_i,2)} \epsilon_{v_j}(0,n_j,0) P^{\min,k_j}_{(l_j,\pm l_j,0),(0,n_j,2)} \\
&\quad \times \prod_{q\neq i,j} \left(P^{k_q}_{(l_q,\pm l_q,0),(0,n_q,0)} \right) \\
&\quad + \sum_{i<j<k<l} \prod_{p=i,j,k,l} \left(\epsilon_{v_p}(0,n_p,0) P^{\min,k_p}_{(l_p,\pm l_p,0),(0,n_p,2)} \right) \\
&\quad \times \prod_{n\neq i,j,k,l} \left(P^{\min,k_q}_{(l_q,\pm l_q,0),(0,n_q,0)} \right) + \cdots \\
&= \prod_{i=1}^{r} \left(P^{\min,k_i}_{(l_i,\pm l_i,0),(0,n_i,0)} \right) \left(1 + \sum_{i<j} \mathrm{i}^2 (-1)^{l_i+l_j} \right. \\
&\quad \left. + \sum_{i<j<k<l} \mathrm{i}^4 (-1)^{l_i+l_j+l_k+l_l} + \cdots \right) \\
&= \mathrm{Re} \left[\prod_{p=1}^{r} (1 + \mathrm{i}(-1)^{l_p}) \right] \prod_{i=1}^{r} \left(P^{\min,k_i}_{(l_i,\pm l_i,0),(0,n_i,0)} \right) \\
&= 2^{(r/2)} \cos(\xi_r) \prod_{i=1}^{r} \left(P^{\min,k_i}_{(l_i,\pm l_i,0),(0,n_i,0)} \right),
\end{aligned}$$

$$
\begin{aligned}
P^r_{[\vec{l};\vec{l}';0],[v][0;\vec{n};0]} &= \epsilon^*_{v_1}(0,n_1,0)\left[\sum_i \epsilon_{v_i}(0,n_i,0) P^{\min,k_i}_{(l_i,\pm l_i,0),(0,n_i,2)}\right. \\
&\quad \times \prod_{q\neq i}\left(P^{\min,k_q}_{(l_q,\pm l_q,0),(0,n_q,0)}\right) \\
&\quad + \sum_{i<j<k}\prod_{p=i,j,k}\left(\epsilon_{v_p}(0,n_p,0)P^{\min,k_p}_{(l_p,\pm l_p,0),(0,n_p,2)}\right) \\
&\quad \left. \times \prod_{n\neq i,j,k}\left(P^{\min,k_q}_{(l_q,\pm l_q,0),(0,n_q,0)}\right) + \cdots\right] \\
&= -\mathrm{i}\prod_{i=1}^{r}\left(P^{\min,k_i}_{(l_i,\pm l_i,0),(0,n_i,0)}\right) \\
&\quad \times \left(\sum_i \mathrm{i}(-1)^{l_i} + \sum_{i<j<k}\mathrm{i}^3(-1)^{l_i+l_j+l_k} + \cdots\right) \\
&= \ \mathrm{Im}\left[\prod_{p=1}^{r}(1+\mathrm{i}(-1)^{l_p})\right]\prod_{i=1}^{r}\left(P^{\min,k_i}_{(l_i,\pm l_i,0),(0,n_i,0)}\right) \\
&= 2^{(r/2)}\sin(\xi_r)\prod_{i=1}^{r}\left(P^{\min,k_i}_{(l_i,\pm l_i,0),(0,n_i,0)}\right), \qquad \text{(B.5)}
\end{aligned}
$$

where we have defined the phase angle,

$$\xi_r \equiv \frac{\pi}{4}\sum_{i=1}^{r}(-1)^{l_i}, \qquad \text{(B.6)}$$

and used $[v][0;\vec{n};0]$ to denote the orbit resulting from the action of the vector current on the Klein Bottle current.

B.2 Models with all k_i even

It can be shown by induction on r that the relevant P-matrix entries of the fermion aligned product of r even k minimal models are

$$P^r_{[\vec{l};\vec{l}';0],[0;\vec{n};0]} \equiv \alpha_r 2^r \cos\left(\theta_r - \frac{\pi r}{4}\right), \qquad \text{(B.7)}$$

$$P^r_{[\vec{l};\vec{l}';0],[v][0;\vec{n};0]} \equiv -\alpha_r 2^r \sin\left(\theta_r - \frac{\pi r}{4}\right), \qquad \text{(B.8)}$$

where we have defined,

$$\theta_r \equiv \sum_{i=1}^{r} \mathrm{i}^{n_i} \frac{\pi(l_i+1)}{2(k_i+2)},$$

$$\alpha_r \equiv \prod_{i=1}^{r} \frac{\mathrm{e}^{(\pi l_i n_i/2(k_i+2))}}{k_i+2}.$$

The induction proof relies on that fact that different theories are fermion aligned by an order two simple current, w, which is the product of the vector currents of each block. First, by expanding out the trigonometric expressions in the P-matrix expressions for the case $r=1$ (B.7) and (B.8), we find agreement with (B.3). Then consider the vector extension of a fermion aligned product of r minimal models (again given by equation (B.7)) and one additional minimal model (given in the form of (B.7) with $r=1$)

$$\begin{aligned}
P^{r+1}_{[\vec{l};l_{r+1};\vec{l}',l'_{r+1};0],[0;\vec{n},n_{r+1};0]} &= P^{r}_{[\vec{l};\vec{l}';0],[0;\vec{n};0]} P^{\min,k_{r+1}}_{(l;l';0),(0;n_{r+1};0)} \\
&\quad + \epsilon_{\vec{v}}([0;\vec{n};0])\epsilon_{v_{r+1}}((0;n_{r+1};0)) P^{r}_{[\vec{l};\vec{l}';0],[v][0;\vec{n};0]} \\
&\quad \times P^{\min,k_{r+1}}_{(l;l';0),(0;n_{r+1};2)} \\
&= \alpha_r 2^r \cos\left(\theta_r - \frac{\pi r}{4}\right) \alpha_1 2 \cos\left(\theta_1 - \frac{\pi}{4}\right) \\
&\quad + (\mathrm{i})^2 \alpha_r 2^r \sin\left(\theta_r - \frac{\pi r}{4}\right) \alpha_1 2 \sin\left(\theta_1 - \frac{\pi}{4}\right) \\
&= 2^{r+1}\alpha_r\alpha_1 \cos\left(\theta_1 + \theta_r - \frac{\pi(r+1)}{4}\right) \\
&= 2^{r+1}\alpha_{r+1} \cos\left(\theta_{r+1} - \frac{\pi(r+1)}{4}\right), \qquad \text{(B.9)}
\end{aligned}$$

in agreement with (B.7). Similarly,

$$\begin{aligned}
P^{r+1}_{[\vec{l};l_{r+1};\vec{l}',l'_{r+1};0],[v][0;\vec{n},n_{r+1};0]} &= P^{r}_{[\vec{l};\vec{l}';0],[v][0;\vec{n};0]} P^{\min,k_{r+1}}_{(l;l';0),(0;n_{r+1};0)} \\
&\quad + \epsilon_{[v]}([v][0;\vec{n};0])\epsilon_{v_{r+1}}((0;n_{r+1};0)) P^{r}_{[\vec{l};\vec{l}';0],[v][0;\vec{n};0]} \\
&\quad \times P^{\min,k_{r+1}}_{(l;l';0),(0;n_{m+1};2)}
\end{aligned}$$

$$
\begin{aligned}
&= -\alpha_r 2^r \sin\left(\theta_r - \frac{\pi r}{4}\right) \alpha_1 2 \cos\left(\theta_1 - \frac{\pi}{4}\right) \\
&\quad - (-\mathrm{i})(\mathrm{i})\alpha_r 2^r \sin\left(\theta_r - \frac{\pi r}{4}\right) \alpha_1 2 \cos\left(\theta_1 - \frac{\pi}{4}\right) \\
&= -2^{r+1}\alpha_r\alpha_1 \sin\left(\theta_1 + \theta_r - \frac{\pi(r+1)}{4}\right) \\
&= -2^{r+1}\alpha_{r+1} \sin\left(\theta_{r+1} - \frac{\pi(r+1)}{4}\right), \qquad \text{(B.10)}
\end{aligned}
$$

again in agreement with the second expression of the (B.8).

B.3 Models with even and odd k

For the generic case of $r = r_\mathrm{e} + r_\mathrm{o}$ even and odd k minimal models we just take the tensor of the even and odd cases that we have studied and fermion align via the order 2 current $w = v_{\mathrm{evenblock}} v_{\mathrm{oddblock}}$. The calculation is similar to (B.9) and (B.10), even to the effect that the ϵ phase factors are also -1 and $+1$. The result is

$$
P^r_{[\vec{l};\vec{l}';0],[0;\vec{n};0]} \equiv \alpha_{r_\mathrm{e}} 2^r \cos\left(\theta_{r_\mathrm{e}} - \frac{\pi r_\mathrm{e}}{4} - \xi_{r_\mathrm{o}}\right) \prod_{i=0}^{r_\mathrm{o}} \frac{1}{\sqrt{2}} P^{\min,k_i}_{(l_i;l'_i;0),((0;n_i;0)}, \qquad \text{(B.11)}
$$

$$
P^r_{[\vec{l};\vec{l}';0],[v][0;\vec{n};0]} \equiv -\alpha_{r_\mathrm{e}} 2^r \sin\left(\theta_{r_\mathrm{e}} - \frac{\pi r_\mathrm{e}}{4} - \xi_{r_\mathrm{o}}\right) \prod_{i=0}^{r_\mathrm{o}} \frac{1}{\sqrt{2}} P^{\min,k_i}_{(l_i;l'_i;0),((0;n_i;0)}. \qquad \text{(B.12)}
$$

B.4 Spacetime extension

Finally we extend with the spacetime WZW theory. The non-zero entries of the P-matrix of $D_{8-n,1}$ are readily computed (see for instance [55]):

$$
\begin{aligned}
P^D_{0,0} &= -P^D_{v,v} = \cos\left(\frac{n\pi}{4}\right), \\
P^D_{0,v} &= -\sin\left(\frac{n\pi}{4}\right), \\
P^D_{s,s} &= P^D_{c,c} = e^{(\mathrm{i}n\pi/4)} \cos\left(\frac{n\pi}{4}\right), \\
P^D_{s,c} &= -\mathrm{i}e^{(\mathrm{i}n\pi/4)} \sin\left(\frac{n\pi}{4}\right). \qquad \text{(B.13)}
\end{aligned}
$$

However, the nature of the extension depends on whether we need the WZW part of the chiral field to be in the vector or in the scalar representation. In particular, the scalar representation is necessary to find the mass/charge

of O-planes. In case the WZW component of the chiral field is the vector primary, we find

$$P^{\rm ws}_{[[\vec{l};\vec{l}';0]v],[[0;\vec{n};0]o]} = P^{r}_{[\vec{l};\vec{l}';0],[0;\vec{n};0]} P^{D}_{v,o} + \epsilon_v(o)\epsilon_{[v]}([0;\vec{n};0]) P^{r}_{[\vec{l};\vec{l}';0],[v][0;\vec{n};0]} P^{D}_{v,v}. \tag{B.14}$$

If it is built on the scalar, then we obtain

$$P^{\rm ws}_{[[\vec{l};\vec{l}';0]o],[[0;\vec{n};0]o]} = P^{r}_{[\vec{l};\vec{l}';0],[0;\vec{n};0]} P^{D}_{o,o} + \epsilon_v(o)\epsilon_{[v]}([0;\vec{n};0]) P^{r}_{[\vec{l};\vec{l}';0],[v][0;\vec{n};0]} P^{D}_{o,v}. \tag{B.15}$$

In both cases the product of the ϵ phase factors equals $+1$. Explicitly we thus obtain

$$P^{\rm ws}_{[[\vec{l};\vec{l}';0]v],[[0,\vec{n},0]o]} = {\rm e}^{{\rm i}\pi\left(a_{[[\vec{l};\vec{l}';0]v]}+a_{[[0,\vec{n},0]o]}\right)} 2^{r_{\rm e}} \alpha_{r_{\rm e}} \sin\left(\theta_{r_{\rm e}} - \frac{\pi}{4}(r_{\rm e}+n) - \xi_{r_{\rm o}}\right) \prod_{i=1}^{r_{\rm o}} \frac{1}{\sqrt{2}} P^{{\rm min},k_i}_{(l_i;l_i';0),(o;n_i;0)}, \tag{B.16}$$

and

$$P^{\rm ws}_{[[\vec{l};\vec{l}';0]o],[[0;\vec{n};0]o]} = {\rm e}^{{\rm i}\pi\left(a_{[[\vec{l};\vec{l}';0]o]}+a_{[[0,\vec{n},0]o]}\right)} 2^{r} \alpha_{r_{\rm e}} \cos\left(\theta_{r_{\rm e}} - \frac{\pi}{4}(r_{\rm e}+n) - \xi_{r_{\rm o}}\right) \prod_{i=1}^{r_{\rm o}} \frac{1}{\sqrt{2}} P^{{\rm min},k_i}_{(l_i;l_i';0),(o;n_i;0)}. \tag{B.17}$$

Here we have reintroduced the phase prefactor, equal to ± 1, which encodes the difference in conformal weights of the true orbit field and that of the representative element chosen for the calculation. As mentioned earlier in the paper, the true weight of the orbit is the smallest of the weights of the representative elements modulo 2.

C Mirror symmetry extension map

From the CFT perspective the difference between the A-type theory and its mirror is that one is based on a diagonal bulk modular invariant while the other is based on the conjugation one. Simple current technology allows us to build all but the most exotic modular invariants. In particular, we can find a set of fields which can supplement the GSO and fermion aligning currents to produce the mirror symmetric theory. The mirror symmetry extension currents are essentially the conjugating fields available after GSO projection.

For a single minimal model conjugation is done through the phase symmetry maps, $p_i = (0,2,0)_i$ of order $k_i + 2$ and weight $h_{p_i} = -1/(k_i+2) \bmod 1$.

As the conformal weight times the order is integer we can use the group generated by this field to construct a modular extension invariant. In the more general Gepner case, the simple current group, $G_{\rm ms}$, of mirror symmetry extension currents is generated by some product of phase symmetry maps $\Pi_{i=1}^r p_i^{\alpha_i}$. We will find constraints on the vector $\vec{\alpha}$ based on the requirement that we have a proper simple current modular invariant and that the simple current preserves the GSO projection of the initial (pre-mirror) theory.

Generally, to construct a simple current modular invariant we need to choose a pairing X [15, 35, 50, 51]. This is a bihomomorphism, $X : G \times G \to \mathbb{R}$, which must satisfy, $X + X^T(g, f) = Q_g(f)$ mod 1, for non-diagonal elements $g, f \in G$. On diagonal elements one requires that $X(g, g) = -h_g$ mod 1. Different solutions for X differ in half integer values in the off-diagonal components.

In this case, we opt for the simplest solution which will yield a conjugate modular invariant. Define $X(p_i, p_j) = \delta_{ij}/(k_i + 2)$. The simple current modular invariant is

$$Z_G = \sum_{\lambda,\kappa} Z_{\lambda,\kappa} \chi_\kappa \bar{\chi}_\lambda, \tag{C.1}$$

where $Z_{\lambda,\kappa}$ is an integer that counts the number of solutions to

$$\begin{aligned} \lambda &= J\kappa, \quad J \in G, \\ Q_g(\kappa) + X(g, J) &= 0, \quad \forall g \in G. \end{aligned} \tag{C.2}$$

Now let $J = \Pi_{i=1}^r p_i^{\alpha_i}$, $g = \Pi_{i=1}^r p_i^{\beta_i}$ and $\kappa = [\vec{l}; \vec{m}; \vec{s}] f_D$, with $\vec{s}, f_D \in$ NS, then the second condition reads,

$$\sum_{i=1}^{r} \frac{\beta_i m_i}{h_i} + \frac{\beta_i \alpha_i}{h_i} = 0 \quad \forall \vec{\beta}, \tag{C.3}$$

which can be solved by $\alpha_i = -m_i$. Applying this to the equation (C.2) then tells us that the field κ with phases $\vec{m}$ is paired up with a field λ whose phases are $J[\vec{l}; \vec{m}; \vec{s}] f_D = [\vec{l}; \vec{m} - 2\vec{\alpha}; \vec{s}] f_D = [\vec{l}; -\vec{m}; \vec{s}] f_D$ as desired for a conjugate field in the NS sector.

This result is not surprising as orbifolding/simple current extending the minimal model by the phase symmetry p yields its conjugate. However, in order to construct a spacetime supersymmetric theory we need to GSO project. We must make sure that the currents we are extending by are admissible in the GSO projected theory. The GSO projection drops all fields with non-integer monodromy charge under the spectral flow, s, so we require that admissible mirror extending currents satisfy the compatibility

condition $Q_s(J) = 0$, or, explicitly,

$$\sum_{i=1}^{r} \frac{\alpha_i}{h_i} = 0. \tag{C.4}$$

In the orbifold language this is equivalent to requiring that the twisted sectors (in the Gepner model) are uncharged with respect to the GSO map.

For the NS case, no further conjugation is necessary. In the Ramond sector, we need to conjugate the values of s_i as well as the spacetime spinor component. This conjugation depends on the parity of n and r as this determines whether the sector is self conjugate or not. The spacetime factor $D_{8-n,1}$ is self conjugate for n even. For n odd, we can extend by v_D to conjugate. Because of fermion alignment the action of v_D is equivalent to the use of v_1. Overall this yields a factor of the form v_1^n. In the Gepner sector, we need to flip the individual s_i values from 1 to -1 and vice versa. If r is even then these two states are equivalent modulo fermion alignment — so the Gepner sector is self conjugate. If the Gepner sector is not self conjugate, then conjugation can be achieved through v_1. Overall we see that the conjugation of the internal sector requires an extensions by v_1^r. Combining the results for the internal Gepner and the spacetime fermion sector we see that we we need to extend by $v_D^n v_1^r$ which is equal to v_1^{n+r} modulo fermion alignment.

We conclude that the Mirror Symmetry extension map is of the form

$$J = v_1^{(n+r)\epsilon} \prod_{i=1}^{r} p_i^{\alpha_i}, \tag{C.5}$$

where ϵ is either 0 or 1 and distinguishes between the NS and R sectors. However, as before, we must make sure that these currents are compatible with the GSO projection. In particular we need,

$$\begin{aligned} Q_s(J) &= 0 \bmod 2 \\ &= \sum \frac{\alpha_i}{h_i} + \frac{(n+r)\epsilon}{2}, \end{aligned} \tag{C.6}$$

so that the mirror symmetry extension currents are neutral with respect to the GSO current.

C.1 Summary

The mirror map is generated by elements of the form

$$G^{\text{Mirror}} = \left\{ v_D^{(n+r)\epsilon} \Pi_{r=1}^{r} p_i^{\alpha_i}, \sum_{i=1}^{r} \frac{\alpha_i}{h_i} - \frac{(n+r)\epsilon}{2} = 0 \bmod 1, \quad \epsilon \in \{0,1\} \right\}, \tag{C.7}$$

with pairing

$$X(p_i, p_j) = \frac{\delta_{ij}}{k_i + 2}. \tag{C.8}$$

C.2 Sample mirror symmetry extension calculation

To illustrate the mirror symmetry extension and the calculation of the sign constraints, we will compute the B-type crosscap coefficients for the Gepner (1,1,1) model $K = (-2, 2, 2)$. The mirror symmetry is generated by the order 3 current $J = p_1 p_2^3$ with conformal weight $h_J = 1/3$. The action of J on the Klein bottle current is

$$\begin{array}{ccccccc} \text{J:}(-2,2,2) & \longrightarrow & (0,0,2) & \longrightarrow & (2,-2,2) & \longrightarrow & (-2,2,2) \\ h_K = 1 & & h_{JK} = 2/3 & & h_{J^2K} = 1 & & \\ \beta_0 = \sigma_0 & & \beta_J = \sigma(JK)\mathrm{e}^{\mathrm{i}\pi/3} & & \beta_{J^2} = \sigma(J^2K)\mathrm{e}^{\mathrm{i}\pi/3} & & \end{array}$$

There are three constraint equations

$$\beta_0 = \sigma_0 = \beta_J \beta_{J^2} \mathrm{e}^{\mathrm{i}2\pi X(J,J^2)} = -\sigma(JK)\sigma(J^2K), \tag{C.9}$$

$$\beta_J = \sigma(JK)\mathrm{e}^{\mathrm{i}\pi/3} = \beta_{J^2}\beta_{J^2}\mathrm{e}^{\mathrm{i}2\pi X(J^2,J^2)} = -\sigma(JK)^2 = -1, \tag{C.10}$$

$$\beta_J^2 = \sigma(J^2K)\mathrm{e}^{\mathrm{i}\pi/3} = \beta_J\beta_J\mathrm{e}^{\mathrm{i}2\pi X(J,J)} = \sigma(J^2K)^2 = 1, \tag{C.11}$$

where we have used that

$$\beta_{J^{n+m}} = \beta_{J^n}\beta_{J^m}\mathrm{e}^{\mathrm{i}2\pi X(Jn2,J^m)}, \tag{C.12}$$

$$\mathrm{e}^{\mathrm{i}2\pi X(Jn2,J^m)} = \mathrm{e}^{-\mathrm{i}2\pi nmh_J}. \tag{C.13}$$

Hence the signs are

$$\sigma_0 = 1, \tag{C.14}$$

$$\sigma(JK) = -1, \tag{C.15}$$

$$\sigma(J^2K) = 1. \tag{C.16}$$

Note that $JK = (0, 0, 2)$ is equivalent to $(2, 2, -2)$ under the $S^2 = (2, 2, 2)$ GSO identification. We would then expect $\sigma(J, K)$ to equal $\sigma(0, K)$ as

JK has the same minimal model components as K modulo permutation. This discrepancy is compensated by a sign difference between $P^{\rm ws}_{(0,0,2),\chi}$ and $P^{\rm ws}_{(2,2,-2),\chi}$. The difference in sign in the P-matrix is in turn given by the choice of $(0,0,2)$ versus $(2,2,-2)$ as representative elements of the S orbit of K. Recall that the prescription is to choose the element with lowest conformal weight mod 1. Had we had done that, it is clear that the computation of the signs would have been trivial, as for this Klein bottle, J maps identical Klein bottle currents K (modulo minimal model permutation) to themselves. As a result the mirror map results in an overall scaling by $\sqrt{3}$.

References

[1] E.G. Gimon and J. Polchinski, *Consistency Conditions for Orientifolds and D-Manifolds*, Phys. Rev. **D54** (1996), 1667, arXiv:hep-th/9601038.

[2] M.R. Douglas, *The statistics of string-/M-theory vacua*, JHEP **05** (2003), 046, `hep-th/0303194`.

[3] S. Kachru *et al.*, *Towards inflation in string theory*, JCAP **0310** (2003), 013, `hep-th/0308055`.

[4] S. Kachru, R. Kallosh, A. Linde and S. P. Trivedi, *De Sitter vacua in string theory*, Phys. Rev. **D68** (2003), 046005, `hep-th/0301240`.

[5] J.J. Blanco-Pillado *et al.*, *Racetrack inflation*, JHEP **11** (2004), 063, `hep-th/0406230`.

[6] C.P. Burgess, J.M. Cline, H. Stoica and F. Quevedo, *Inflation in realistic d-brane models*, JHEP **09** (2004), 033, `hep-th/0403119`.

[7] T.P.T. Dijkstra, L.R. Huiszoon and A.N. Schellekens, *Chiral supersymmetric standard model spectra from orientifolds of gepner models*, Phys. Lett. **B609** (2005), 408–417, `hep-th/0403196`.

[8] C.V. Johnson, A.W. Peet and J. Polchinski, *Gauge theory and the excision of repulson singularities*, Phys. Rev. **D61** (2000), 086001, `hep-th/9911161`.

[9] D. Marolf and S.F. Ross, *Stringy negative-tension branes and the second law of thermodynamics*, JHEP **04** (2002), 008, `hep-th/0202091`.

[10] A. Sen, *Orientifold limit of F-theory vacua*, Phys. Rev. **D55** (1997), 7345–7349, `hep-th/9702165`.

[11] A. Sen, *F-theory and the Gimon-Polchinski orientifold*, Nucl. Phys. **B498** (1997), 135–155, `hep-th/9702061`.

[12] A. Sen, *A non-perturbative description of the Gimon-Polchinski orientifold*, Nucl. Phys. **B489** (1997), 139–159, `hep-th/9611186`.

[13] N. Seiberg and E. Witten, *Gauge dynamics and compactification to three dimensions*, `hep-th/9607163`.

[14] J. Polchinski, *Tensors from K3 orientifolds*, Phys. Rev. **D55** (1997), 6423–6428, `hep-th/9606165`.

[15] L.R. Huiszoon, *D-branes and O-planes in string theory: An algebraic approach*, Ph.D. thesis, NIKHEF, 2002.

[16] T.P.T. Dijkstra, L.R. Huiszoon and A.N. Schellekens, *Supersymmetric standard model spectra from RCFT orientifolds*, Nucl. Phys. **B710** (2005), 3–57, `hep-th/0411129`.

[17] R. Blumenhagen, M. Cvetic, P. Langacker, and G. Shiu, *Toward realistic intersecting D-brane models*, `hep-th/0502005`.

[18] R. Blumenhagen and A. Wisskirchen, *Spectra of 4d, N = 1 type I string vacua on non-toroidal CY-threefolds*, Phys. Lett. **B438** (1998), 52–60, `hep-th/9806131`.

[19] C. Schmidhuber, *D-brane actions*, Nucl. Phys. **B467**, (1996), 146, arXiv:hep-th/9601003.

[20] B. Acharya, M. Aganagic, K. Hori and C. Vafa, *Orientifolds, mirror symmetry and superpotentials*, `hep-th/0202208`.

[21] R. Blumenhagen, V. Braun, B. Kors and D. Lust, *Orientifolds of K3 and Calabi–Yau manifolds with intersecting D-branes*, JHEP **07** (2002), 026, `hep-th/0206038`.

[22] D.-E. Diaconescu, B. Florea, and A. Misra, *Orientifolds, unoriented instantons and localization*, JHEP **07** (2003), 041, `hep-th/0305021`.

[23] A. Misra, *Type IIA on a compact Calabi–Yau and d = 11 supergravity uplift of its orientifold*, Fortsch. Phys. **52** (2004), 831–870, `hep-th/0311186`.

[24] A. Misra, *On (orientifold of) type IIA on a compact Calabi–Yau*, Fortsch. Phys. **52** (2004), 5–27, `hep-th/0304209`.

[25] A. Misra, *MQCD, ('barely') G(2) manifolds and (orientifold of) a compact Calabi–Yau*, Int. J. Mod. Phys. **A20** (2005), 2059–2098, `hep-th/0403012`.

[26] S. Govindarajan and J. Majumder, *Orientifolds of type IIA strings on Calabi–Yau manifolds*, Pramana **62** (2004), 711–716, `hep-th/0305108`.

[27] S. Govindarajan and J. Majumder, *Crosscaps in Gepner models and type IIA orientifolds*, JHEP **02** (2004), 026, `hep-th/0306257`.

[28] I. Brunner and K. Hori, *Orientifolds and mirror symmetry*, JHEP **11** (2004), 005, `hep-th/0303135`.

[29] I. Brunner, K. Hori, K. Hosomichi and J. Walcher, *Orientifolds of Gepner Models*, `hep-th/0401137`.

[30] I. Brunner and K. Hori, *Notes on orientifolds of rational conformal field theories*, JHEP **07** (2004), 023, `hep-th/0208141`.

[31] R. Blumenhagen, *Supersymmetric orientifolds of Gepner models*, JHEP **11** (2003), 055, `hep-th/0310244`.

[32] R. Blumenhagen and T. Weigand, *Chiral supersymmetric Gepner model orientifolds*, JHEP **02** (2004), 041, `hep-th/0401148`.

[33] G. Aldazabal, E.C. Andres, M. Leston and C. Nunez, *Type IIB orientifolds on Gepner points*, JHEP **09** (2003), 067, `hep-th/0307183`.

[34] J. Fuchs, C. Schweigert and J. Walcher, *Projections in string theory and boundary states for Gepner models*, Nucl. Phys. **B588** (2000), 110–148, `hep-th/0003298`.

[35] J. Walcher, *Worldsheet boundaries, supersymmetry, and quantum geometry*, Ph.D. thesis, ETH Zurich, 2001.

[36] R. Blumenhagen and T. Weigand, *A note on partition functions of Gepner model orientifolds*, Phys. Lett. **B591** (2004), 161–169, `hep-th/0403299`.

[37] N. Alling and N. Greenleaf, *Foundations of the theory of Klein surfaces*, Lect. Notes Math., **219**, Springer, Berlin-Heidelberg-New York, 1971.

[38] N. Alling, *Real elliptic curves*, Mathematics Studies, **54**, North Holland Publishing Company, Amsterdam, New York, Oxford, 1981.

[39] P. Du Val, *Elliptic functions and elliptic curves*, London Math. Soc. Lect. Notes Series, **9**, Cambridge University Press, 1973.

[40] J. Huisman, *Algebraic moduli of real elliptic curves*, Commun. Algebra **29**(8) (2001), 3459–3476.

[41] S. Gukov and C. Vafa, *Rational conformal field theories and complex multiplication*, Commun. Math. Phys. **246**, (2004), 181, arXiv:hep-th/0203213.

[42] J.F. Morales, C.A. Scrucca and M. Serone, *Anomalous couplings for D-branes and O-planes*, Nucl. Phys. B **552**, (1999), **291**, arXiv:hep-th/9812071.

[43] C.A. Scrucca and M. Serone, *Anomalies and inflow on D-branes and O-planes*, Nucl. Phys. B **556**, (1999), **197**, arXiv:hep-th/9903145.

[44] B.R. Greene, *String theory on Calabi–Yau manifolds*, `hep-th/9702155`.

[45] D. Gepner, *Space-time supersymmetry in compactified string theory and superconformal models*, Nucl. Phys. **B296** (1989), 757.

[46] A. Casher, F. Englert, H. Nicolai and A. Taormina, *Consistent superstrings as solutions of the d = 26 bosonic string theory*, Phys. Lett. **B162** (1985), 121.

[47] A. Schellekens, *Multiloop modular invariance of the covariant lattice construction of fermionic strings*, Phys. Lett. **B199** (1987), 427.

[48] W. Lerche, A.N. Schellekens and N.P. Warner, *Lattices and strings*, Phys. Rept. **177** (1989), 1.

[49] L.R. Huiszoon and K. Schalm, *BPS orientifold planes from crosscap states in Calabi–Yau compactifications*, JHEP **11** (2003), 019, `hep-th/0306091`.

[50] A.N. Schellekens and S. Yankielowicz, *Simple currents, modular invariants and fixed points*, Int. J. Mod. Phys. **A5** (1990), 2903–2952.

[51] A.N. Schellekens and S. Yankielowicz, *Extended chiral algebras and modular invariant partition functions*, Nucl. Phys. **B327** (1989), 673.

[52] J. Fuchs *et al.*, *Boundary fixed points, enhanced gauge symmetry and singular bundles on $K3$*, Nucl. Phys. **B598** (2001), 57–72, `hep-th/0007145`.

[53] J. Fuchs, L.R. Huiszoon, A.N. Schellekens, C. Schweigert and J. Walcher, *Boundaries, crosscaps and simple currents*, Phys. Lett. B **495**, (2000), 427, arXiv:hep-th/0007174.

[54] G. Pradisi, *Open superstrings*, Nuovo Cim. **B112** (1997), 467–483, `hep-th/9603104`.

[55] C. Angelantonj and A. Sagnotti, *Open strings*, Phys. Rept. **371** (2002), 1–150, `hep-th/0204089`.

[56] A. Sagnotti and Y.S. Stanev, *Open descendants in conformal field theory*, Fortsch. Phys. **44** (1996), 585–596, `hep-th/9605042`.

[57] N. Ishibashi, *The boundary and crosscap states in conformal field theories*, Mod. Phys. Lett. **A4** (1989), 251.

[58] J.L. Cardy, *Boundary conditions, fusion rules and the verlinde formula*, Nucl. Phys. **B324** (1989), 581.

[59] G. Pradisi, A. Sagnotti and Y.S. Stanev, *Planar duality in SU(2) WZW models*, Phys. Lett. **B354** (1995), 279–286, `hep-th/9503207`.

[60] J. Fuchs and C. Schweigert, *Symmetry breaking boundaries. I: General theory*, Nucl. Phys. **B558** (1999), 419–483, `hep-th/9902132`.

[61] J. Fuchs and C. Schweigert, *Symmetry breaking boundaries. II: More structures, examples*, Nucl. Phys. **B568** (2000), 543–593, `hep-th/9908025`.

[62] L.R. Huiszoon, A.N. Schellekens, and N. Sousa, *Klein bottles and simple currents*, Phys. Lett. **B470** (1999) 95–102, `hep-th/9909114`.

[63] I. Brunner, M.R. Douglas, A.E. Lawrence and C. Romelsberger, *D-branes on the quintic*, JHEP **0008**, (2000), 015, arXiv:hep-th/9906200.

[64] W. Lerche, C. Vafa, and N.P. Warner, *Chiral rings in N=2 superconformal theories*, Nucl. Phys. **B324** (1989), 427.

[65] P. Di Vecchia and A. Liccardo, *D-branes in string theory. I*, NATO Adv. Study Inst. Ser. C. Math. Phys. Sci. **556** (2000), 1–59, `hep-th/9912161`.

[66] P. Di Vecchia and A. Liccardo, *D-branes in string theory. II*, `hep-th/9912275`.

[67] P. Di Vecchia *et al.*, *Classical p-branes from boundary state*, Nucl. Phys. **B507** (1997), 259–276, `hep-th/9707068`.

[68] J. Callan, G. Curtis, C. Lovelace, C.R. Nappi and S.A. Yost, *Loop corrections to superstring equations of motion*, Nucl. Phys. **B308** (1988), 221.

[69] V. Nikulin, *Involutions of integer quadratic forms and their applications to real algebraic geometry*, Izv. Akad. Nauk. SSSR Ser. Mat. **47**(1) (1988), 109–188.

[70] R. Silhol, *Real Algebraic Surfaces*, Lect. Notes Maths., **1392**, Springer, Berlin-Heidelberg-New York, 1989.

[71] A. Degtyarev, I. Itenberg and V. Kharlamov, *Real Enriques Surfaces*, vol. 1746 of Lecture Notes in Mathematics. Springer, Berlin-Heidelberg-New York, 2000.

[72] C. Doran, *Picard-fuchs uniformization: modularity of the mirror map and mirror-moonshine*, Centre de Recherches Mathématiques, CRM Proc. Lect. Notes **24** (2000).

[73] S. Herfurtner, *Elliptic surfaces with four singular fibers*, Mathematische Annalen **291** (1991), 319–342.

[74] B. Lian and S. Yau, *Arithmetic properties of mirror map and quantum coupling*, Commun. Math. Phys. **176** (1996), 163–193.

[75] D. Lust, S. Reffert, E. Scheidegger and S. Stieberger, *Resolved toroidal orbifolds and their orientifolds*, arXiv:hep-th/0609014.